sciendo

Contributions to Geophysics and Geodesy Vol. 48/4, 2018 (281–298)

Structural setting of the Koum sedimentary basin (north Cameroon) derived from EGM2008 gravity field interpretation

Yves SHANDINI[1,2], Patrice Arnaud KOUSKE[3], Severin NGUIYA[4], Mouzong Pemi MARCELIN[1,5]

[1] Department of Physics, Faculty of Science, University of Yaounde I, Cameroon

[2] Department of Oceanology and Limnology, Institute of Fisheries and Aquatic Sciences at Yabassi, The University of Douala, Cameroon; e-mail: shandiniyves@gmail.com

[3] Institute of technology, University of Douala, Cameroon; e-mail: arnaudpatricek@yahoo.fr

[4] Faculty of Industrial Engineering, University of Douala, Cameroon; e-mail: nguiyaplus@yahoo.fr

[5] Higher Technical Teacher's Training College, Department of Renewable energy, University of Buea, Cameroon; e-mail: mouzong.pemi@ubuea.cm

Abstract: This study is a contribution to the planning of hydrocarbon exploration program of the Koum sedimentary basin in North Cameroon. 3D modeling of WGM2012 gravity data derived from EGM2008 geopotential model in the Koum basin was used together with existing geological and spectral analysis information to give structural picture of the basin. The 3D model of the Koum basin confirms that the basin is developed as a half graben bounded by sub-vertical faults. The thickness of the Cenozoic sediments is about 1.5 km in the eastern part and reaches 4.5 km in the western part of the basin. Gravity lineaments computed by multi-scale analysis revealed structural trends in the E–W, NW–SE, NE–WS and N–S directions. The faults in the sedimentary terrain reach 6 km depth and have a predominant NW–SE trend with E–W trending faults along the contact between the sedimentary section and the basement complex in the northern edge.

Key words: Koum sedimentary basin, 3D density model, spectral analysis, horizontal gradient, faults

1. Introduction

In view of investigating new sources of oil and gas, Cameroon envisages to conduct exploration of hydrocarbon resources of onshore sedimentary basins

doi: 10.2478/congeo-2018-0013

(Koum, Mamfe and Garoua). Even though geological and geophysical exploration activities in Cameroon started more than 50 years ago, geology of these basins is relatively unknown compared with the coastal basins. The Koum basin which is the largest of the isolated Cretaceous basins in the north Cameroon region has been poorly studied because of its relative inaccessibility and thus is poorly covered by the country geophysical database.

In this paper we present the subsurface structure setting of the Koum sedimentary basin using gravity data extracted from the World Gravity Map (WGM 2012) database (*Bonvalot et al., 2012; Balmino et al., 2012*) derived from the EGM2008 geopotential model. Gravity method is one of the best geophysical techniques for delineating subsurface structures and is widely used in hydrocarbon exploration to establish the limits and structure of sedimentary basins. In this work, a constrained 3D density model of the upper crust in the Koum basin area was obtained based on Bouguer anomaly data by means of modelling and inversion. Multi-scale analysis was also applied to obtain a map of the geological contacts and deep faults in the area. This study is a contribution to the planning of hydrocarbon exploration program of the Koum basin since the appraisal of the basin subsurface structure can allow the delineation of areas with large sedimentary thickness which are believed to be areas of possible hydrocarbon exploration targets and since, in general, fractures and faults within a reservoir can provide important pathways for the movement of reservoir fluids.

2. Geological and tectonic settings

The Koum basin also called Mayo Rey basin is located in the northern region of Cameroon between latitudes $8^\circ\,11'$ and $8^\circ\,20'$ and longitudes $14^\circ\,11'$ and 15°. The Koum basin stretches over 80 km long by 16 km wide (*Brunet et al., 1988; Brunet et al., 1990; Maurin et al., 1986; Schwoerer, 1965*) and covers a total surface area of about 1200 km^2. The Koum basin is a relatively small half-graben, located about 25 km to the southeast of outcrops of Yola Arm and Benue through (*Popoff, 1988*) (Figs. 1 and 2) filled primarily by sediments of Cretaceous age covered by thin ferruginous hardground and recent alluviums (*Duperon-Laudoueneix, 1991; Brabant, 1976; Brabant and Gavaud, 1985*). *Popoff (1988)* proposed that the Koum basin were part of

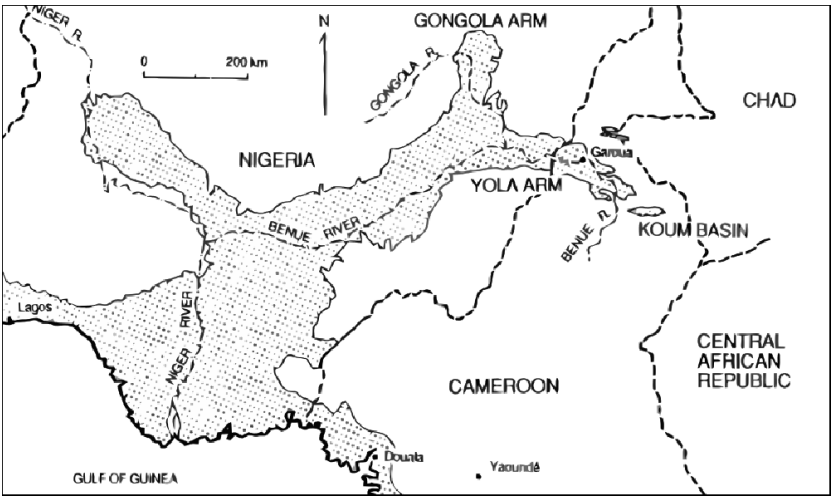

Fig. 1. Distribution of cretaceous and younger sediments in the Benue trough (after *Allix and Popoff, 1983*).

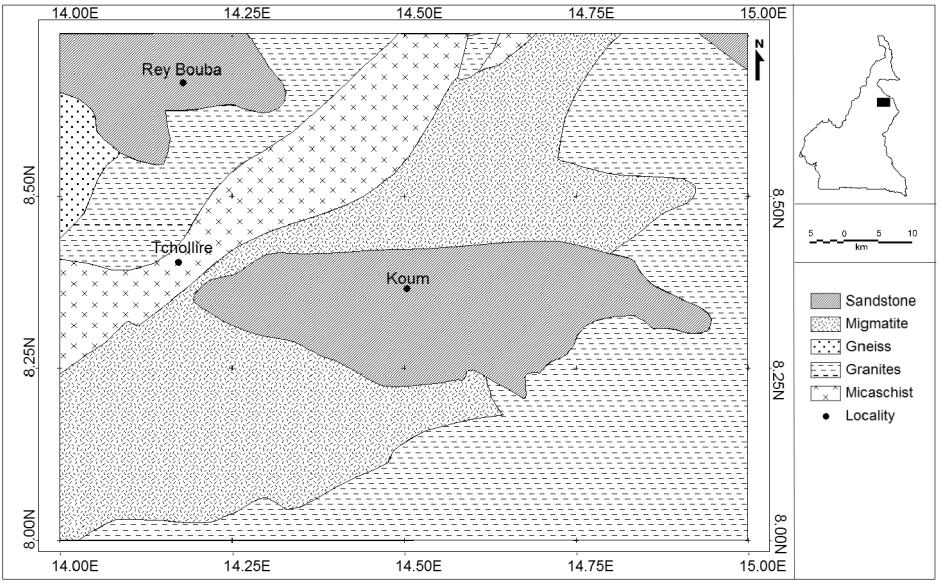

Fig. 2. Geological sketch map of the Koum basin.

an early episode of rifting associated with N–S extensional regime which existed prior to inception of the Benue trough proper. *Brunet et al. (1990)* also implicate the Koum basin in an early episode of rifting which preceded the formation of the main part of the Benue trough. The geologic map of *Schwoerer (1965)* shows Yola Arm sediments to be similar in age to those in the Koum basin. He grouped the Koum basin rocks with those of the Logone and Benoue Basins, defining their age as "Cretace Moyen".

3. Database and gravity field features

The Bouguer gravity data for the study area has been acquired from the World Gravity Map (WGM 2012) database (*Bonvalot et al., 2012; Balmino et al., 2012*). WGM 2012 gravity data is available all over the globe, has no gaps and therefore can provide suitable data for geological and geophysical applications in areas lacking surface gravity measurements. The WGM 2012 Bouguer data is derived from the EGM2008 geopotential model (*Pavlis et al., 2012*) and is computed at the Earth's surface with a $1' \times 1'$ resolution. The EGM2008 geopotential model was developed by the National Geospatial-Intelligence Agency (NGA) and includes surface gravity measurements (from land, marine or airborne surveys), satellite altimetry and satellite gravimetry (GRACE mission) measurements. Technical specifications on EGM 2008 gravity fields can be found in National Geospatial-Intelligence Agency (NGA) website: `http://earth-info.nga.mil/GandG/wgs84/gravitymod/egm2008`.

The available WGM 2012 Bouguer gravity data of the Koum area is presented as a 5 mGal contour map (Fig. 3). The reference density used for the Bouguer anomaly map of the study area is 2670 kg/m^3 and projection information: UTM, zone 33, spheroid and datum WGS 84.

In situ Bouguer gravity data of the survey area (*Collignon, 1968*) have been extracted from the ORSTOM (Office de la Recherche Scientifique et Technique Outre-Mer) database and compared with the Bouguer gravity data generated using EGM2008. The raw gravity data study was acquired with the Worden or Lacoste and Romberg gravimeters with a resolution of 0.01 mGal. They were collected at about 4 km intervals between gravity stations, on all available roads and tracks in the area (Fig. 3). All

gravity measurements were tied to the International Gravity Standardization Network 1971 (IGSN71) datum after correction of luni-solar effect and instrumental drift. The measurement accuracy was about 0.5 mGal. To determine the Free-Air anomaly, the linear vertical gradient of 0.3086 mGal/m was used to approximate free-air correction. Elevation values were obtained with Wallace and Tiernan altimeters. A correction density of 2670 kg/m^3 was used for the Bouguer correction. The statistics of the differences of *in situ* and EGM2008 Bouguer gravity anomalies for the study area are given in Table 1.

Table 1. *In situ* vs EGM2008 Bouguer gravity data differences.

Number of values	129
Minimum	3.66 mGal
Maximum	26.93 mGal
Mean	14.51 mGal
Standard deviation	3.59 mGal

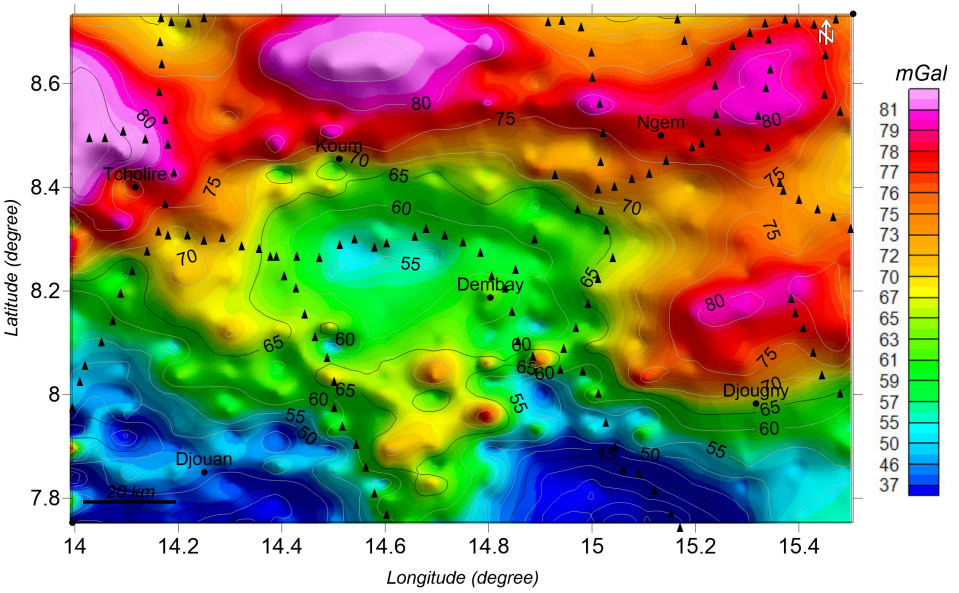

Fig. 3. Bouguer Gravity map of the Koum area. Black triangles show the ground gravity stations.

On the Bouguer gravity map, the Cenozoic sediments of Koum basin are characterized by a long-wavelength gravity low which reaches a minimum value of 55 mGal in the central part of the Bouguer map. The northern, western and eastern parts of the map show gravity highs of about 82 mGal associated to Precambrian basement rocks. The southern area of the map is characterized by gravity lows reaching 35 mGal. The southern negative anomalies don't correlate with surface geology (granite bodies and metamorphic rocks) and thus can be interpreted as gravitational effect of a deep tectonic depression in the southern part of the basin. The central negative anomaly is bounded by relatively steep gradients in the northern, western and eastern edges. It can be inferred that the Koum basin is a half graben bounded by faults in the northern, western and eastern edges.

4. Bouguer anomaly regional/residual separation

This study is based on qualitative and quantitative analysis of the Bouguer gravity data to delineate basement structure of the Koum basin area. Regional/Residual separation was made using polynomial method to isolate deep source from shallow sources. Zeng's technique (*Zeng, 1989*) was applied to determine the degree of the polynomial that gives the most efficient estimation of the regional trend from the Bouguer anomaly data. To apply the Zeng's technique:

- Bouguer gravity data were upward-continued at different levels by step of 5 km up to 60 km and the number of extremes counted,
- the number of extremal points of the calculated upward continuation map was plotted against the corresponding level of continuation (Fig. 4a). From Fig. 4a, it is seen that, for $h \geq 25$ km, the number of extreme points of the anomaly contour map at different heights is approximately constant.

The polynomials of degree $1, 2, \ldots, 10$ have been fitted to the upward continuation map at height $h_m = 25$ km and as a result, a graph of variance against the polynomial degree is plotted (Fig. 4b). The optimum upward continuous height of 25 km obtained to determine the regional trend from

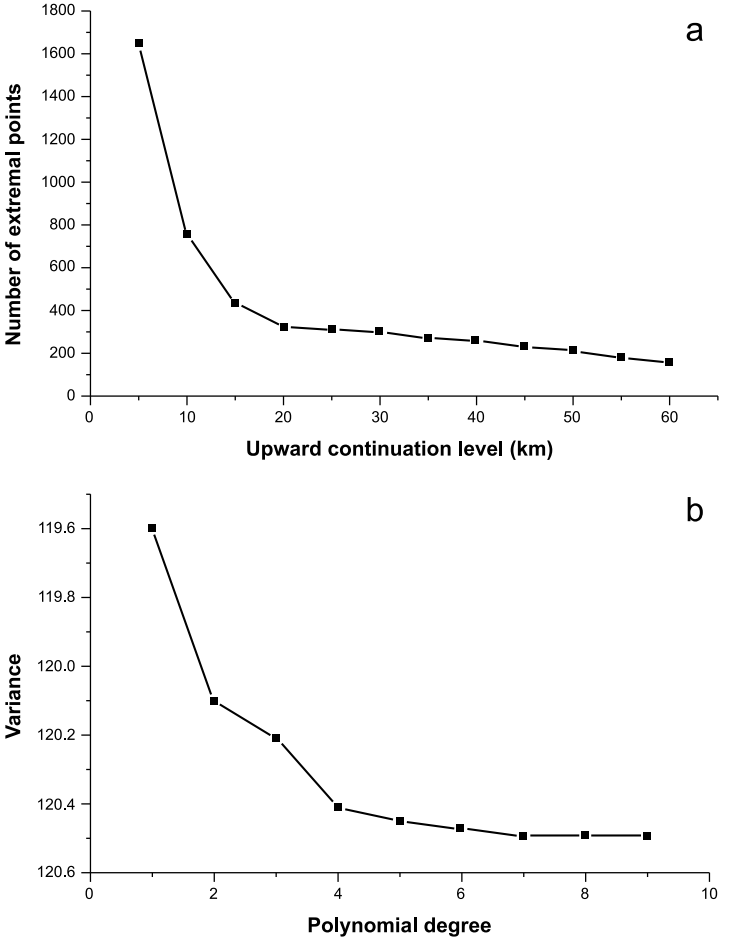

Fig. 4. a) graph of variation of the number of extrema according to the upward continuation height, b) graph of the variance according to the degree of the polynomial.

the Bouguer anomaly data is consistent with the results of deep seismic investigations by *Tokam et al. (2010)* who find a crustal thickness of 25.5 km in the South of Yola through. The appropriate degree of the regional polynomial is estimated from the point of gradient turning point on this graph. Accordingly, the optimum degree of polynomial representing the upward continuation of the observed anomaly at height $h_m = 25$ km is four.

The regional structure (Fig. 5) is characterized by a gradient decreasing towards the south possibly indicating crustal thickening. The variations on the regional anomaly can be interpreted as the undulations of the Moho. This map indicates that the Mohorovicic discontinuity is rising northward.

The regional component was subtracted from the Bouguer map to obtain the residual map (Fig. 6). On the residual map the gravity low associated to the sedimentary formations is more pronounced and enable to better delimit the extension of the basin with a possible reservation, namely that some part of the gravity signal coming from the basin infill can be still included also in the regional gravity anomaly map which, unfortunately, is and will remain a week point of the polynomial method of regional/residual separation.

5. Tectonic trend analysis

To extract deep faults in the study area, multi-scale edge analysis was performed on WGM2012 Bouguer gravity dataset. Bouguer gravity data were firstly upward-continued at different levels 2, 4, 6, 8, 10 and 12 km. Horizontal gradient maxima of upward-continued data at different levels were calculated and plotted (Fig. 7).

In 2D top view, the linear features defined by the succession of points are related to the trend of the deep faults in the area and these faults are traced along these salient features. The resulting set of lineaments is shown in Fig. 8. The horizontal derivative of gravity anomalies is maximum over the boundaries of geological structures like horst or graben, masses extending horizontally and vertically, fault blocks and volcanic intrusive bodies (*Blakely, 1995*).

The lineaments in the study area are shown in Fig. 8. The basement terrains tend to have the greater number of lineaments than in the sedimentary terrain. The rose diagram for all the lineaments mapped in the study area is shown in Fig. 9. The predominant trends of the lineaments are E–W, NW–SE, NE–WS and N–S. The faults in the sedimentary terrain have a predominant NW–SE trend with E–W trending faults along the contact between the sedimentary section and the basement complex at the latitude of Koum town. The horizontal gradient maxima map in the basin

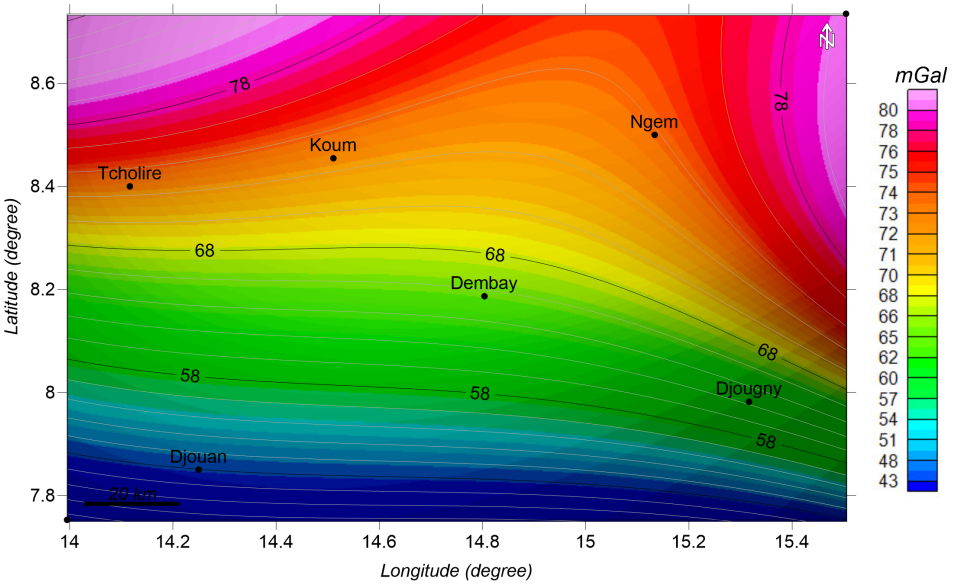

Fig. 5. Regional gravity anomaly map of the Koum area.

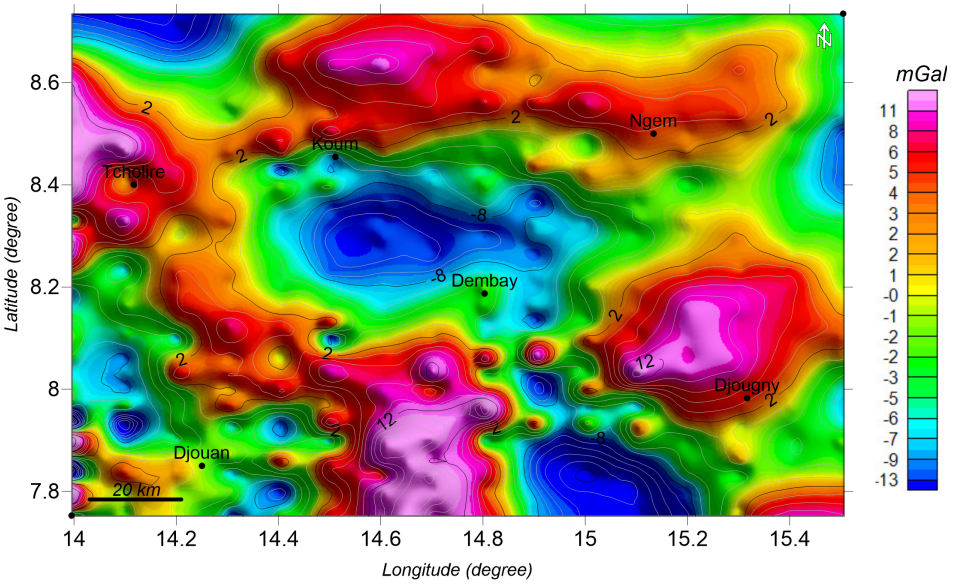

Fig. 6. Residual gravity anomaly map of the Koum area.

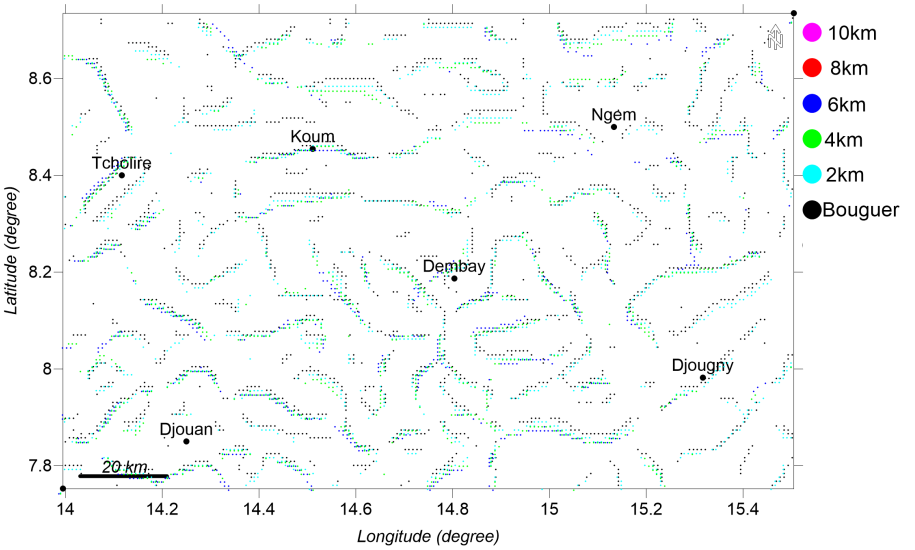

Fig. 7. Horizontal gradient maxima of the residual Bouguer anomaly map and its upward continuations to different heights.

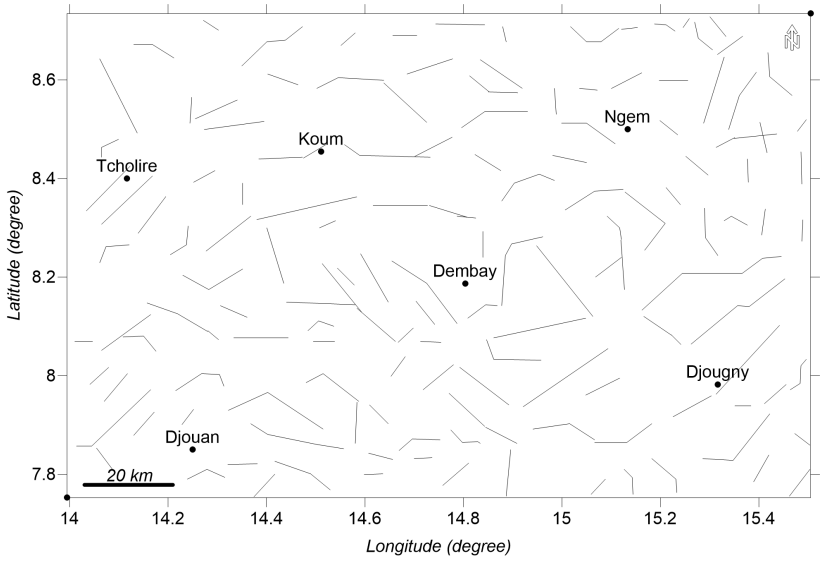

Fig. 8. Lineament map of the study Koum basin area.

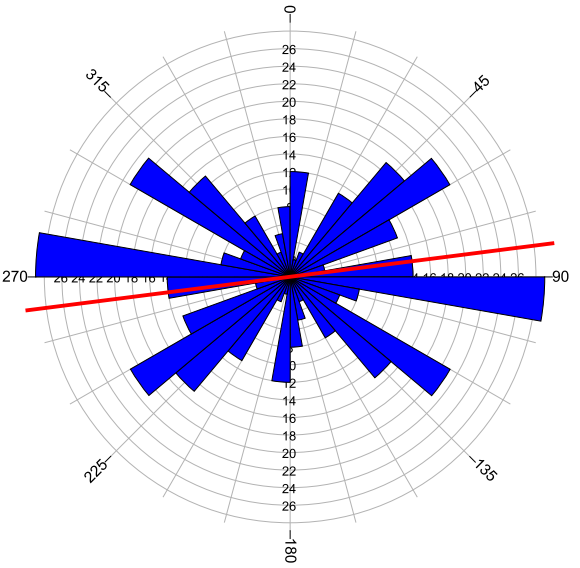

Fig. 9. Tectonic trends derived from Bouguer, regional and residual maps of the study area.

suggest that these faults affect the sediment formations up to 6 km depth. The faults in the basement terrain have a slightly different orientation with predominant NE–SW trend with few NW–SE and E–W directions. The orientation analysis of gravity lineaments shows various tectonic patterns which were found consistent to a great extent with the regional tectonic grain in the upper Benue through (*Ogunmola et al., 2014; 2016*).

6. 3D gravity inversion and modelling

The residual map was used to infer the uppermost crustal density variations in the Koum area by modelling and inversion. The data analysis methodological approach emphasized the integration of geological and geophysical constraints into the forward modeling. For geological constraints, information from the simplified geological map outlining the main superficial lithostratigraphic units was used complemented by borehole data (*Nolla Junior et al., 2015*). Geophysical constraining focused on direct interpretation of the gravity field (power spectrum analysis).

6.1 Power spectrum analysis

In order to compute the maximum sedimentary thickness in the basin, 2-D spectral analysis was carried out on the residual data over central negative anomaly (Fig. 6). FOURPOT 1.3 software (*Pirttijärvi, 2014a*) has been used to calculate the radial amplitude spectrum of the residual as a function of radial wave-number k_r. The residual gravity field values were transformed from the space domain to the frequency domain by means of a Fast Fourier Transform (FFT). Padding and Tapering were applied to remove the Gibbs phenomenon effect as well as ringing and other artifacts in the inverse transformed data and to prevent rapid amplitude changes at the borders of the data area. The power spectrum curve is presented in Fig. 10. On this curve, two straight line segments can be identified and plotted by a least square fitting on the data points. The mean depth of density contrast plane is represented by $h1$ in the low frequency range associated to deep-seated bodies and $h2$ in the high frequency range caused by bodies near surface. The mean depth estimates for the deepest discontinuities obtained is 4.567 km. This depth is related to deep seated bedrock underlying the thick sediment

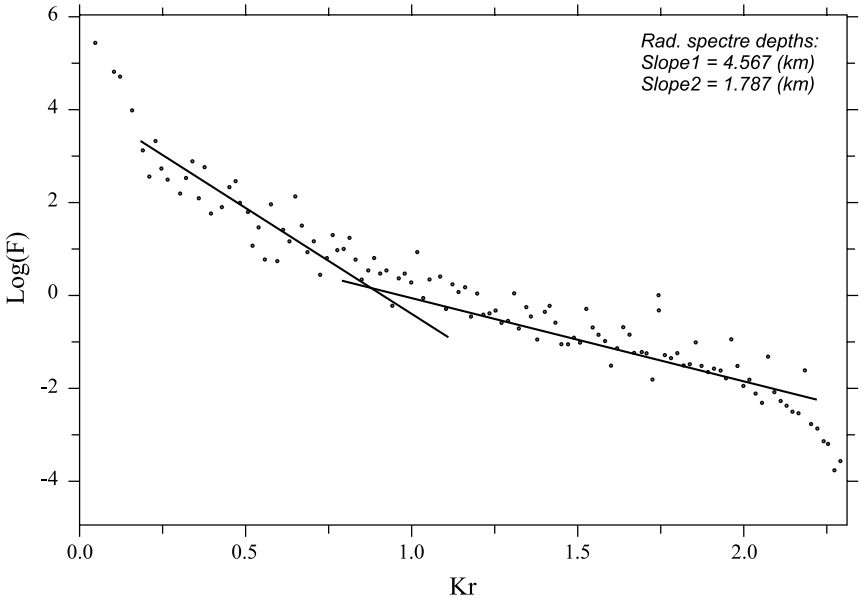

Fig. 10. Power spectrum of the gravity data over the negative central anomaly.

in the area. This result is consistent with those obtained by *Nolla Junior et al. (2015)* who estimated the maximum thickness of sediments in the region at about 4.3 km using field measurements of strikes and dips of beds. The shallowest depths obtained from the second profile is 1.787 km. If we adopt a straightforward approach, this depth should correspond to an intra basin density variation. However, the author of the used software himself (*Pirttijärvi, 2014a*) advised some reserve since the method of depth determination had not been sufficiently verified. A combination of other geophysical techniques or an a-priori geological information would be necessary in order to justify the interpretation suggested here.

6.2 3D density model

For three-dimensional gravity modelling and inversion, the software GRABLOX2 2.1a developed by *Pirttijärvi (2014b)* was used. The main purpose was to optimize the density contrast and/or the shape and dimension of the density variations. GRABLOX computes the synthetic gravity anomaly of a large rectangular super block, which is divided into smaller brick-like volume elements. As the gravity modelling is generally ambiguous, we used depth to the source of the gravity anomaly estimated by spectral analysis in order to constrain gravity modelling. Furthermore, geological constraints (density values) were deduced from the density values (*Kamguia et al., 2005*) and lithostratigraphic studies (*Nolla Junior et al., 2015*) published in the area of study and in surrounding areas.

The starting model was constructed by selecting a $100 \times 300 \times 8$ km super block as the area for density modelling (Fig. 11). The block was discretized by grid blocks of dimension 1.44 km and 1.49 km in the E–W and N–S directions. Constant density values were assigned to each minor individual block. Forward calculation was applied on the measured data to have the computed model, and then Occam inversion method was applied to optimize the density contrast model. The RMS error of the resultant model is 0.481 mGal and the maximum difference between the observed and calculated Bouguer data is 16 mGal. The resultant density model obtained after 7 iterations is shown in multiple layers (Fig. 12). The main features modeled in the central part of the model are lower density bodies (1) with densities ranging from 2.59 to 2.63 g/cm^3. These bodies are related

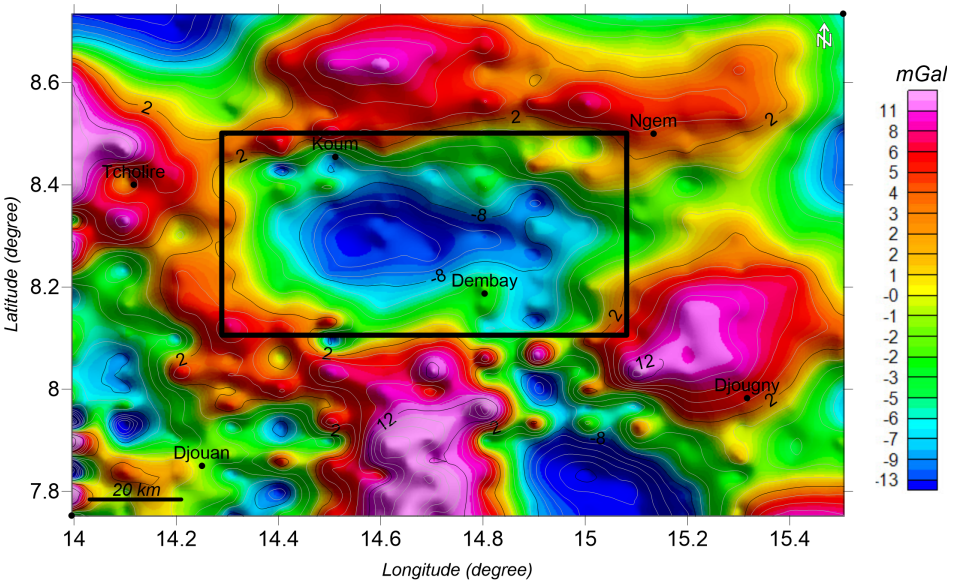

Fig. 11. Plain view of the super block for the comprehensive 3D gravity model of the Koum basin.

to cretaceous sediments. The Koum basin low density zone is characterized by a large horizontal extension in the shallow part and gradually decrease downward in the deeper part. Metamorphic rocks surrounding the basin have densities ranging between 2.64 and 2.7 g/cm^3. Obviously, none of the bodies is expected to really have a homogenous density, because of both the presence of lithologic alternations and the natural increasing of density with depth.

A 2D cross section A–B through the 3D model (Fig. 13) shows that the sediment thickness under the eastern part of the basin is shallower than in the western part. It is about 1.5 km beneath the eastern part and reach more than 4 km in deepest western area.

7. Conclusion

In this paper, we attempted to give an insight on the structural setting of the Koum sedimentary basin using WGM2012 gravity data. Regional and

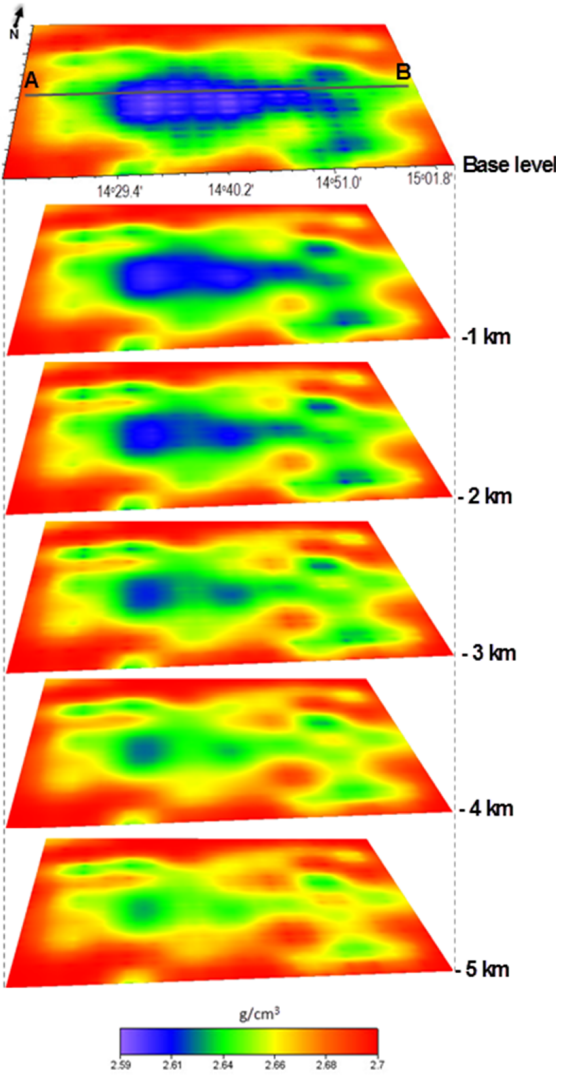

Fig. 12. Resulted 3D gravity inversion maps of the study area.

residual components were separated using the polynomial fitting technique. 3D Modeling of the gravity indicates the sediment thickness is about 1.5 km in the eastern part of the basin and gets deeper in the eastern part to reach 4.5 km. Multi-scale analysis was applied to the residual data and results

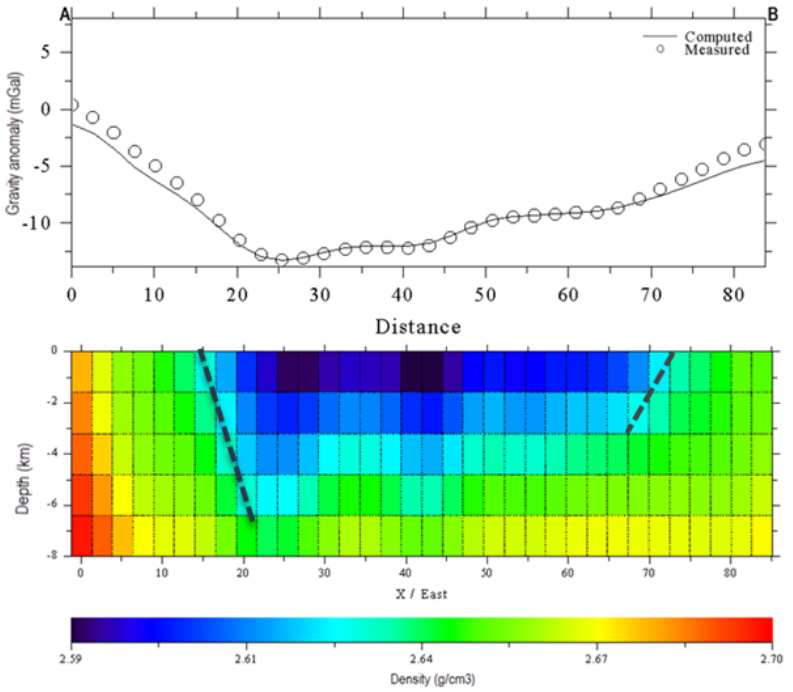

Fig. 13. 2D gravity inversion section across profile A–B.

show that the NW–SE and E–W trends characterize the structure setting of the Koum basin area. The results of this study can be employed as a cost-effective tool for delineating preliminary locations for more sophisticated and more expensive geophysical and/or geochemical surveys in the Koum basin.

Acknowledgements. We thank the National Geospatial-Intelligence Agency (NGA) for compiling and making available the dataset used in this work. We are also thankful to Dr. Ján Mikuška for his suggestions to improve the manuscript.

References

Allix P., Popoff M., 1983: Le Crétacé inférieur de la partie nord-orientale do fossé de la Bénoué (Nigeria) un exemple de relation étroite entre tectonique et sédimentation.

In: Popoff M. and Tiercelin J. J. (Eds.): Rifts et Fossés Anciens: Tectonique-volcanisme-sédimentation, apports de l'actualisme. Table ronde du centre National de la recherche Scientifique (Marseille, 1982). Bulletin des Centres de Recherches Exploration-Production Elf-Aquitaine, **7**, 1, 349–359 (in French).

Balmino G., Vales N., Bonvalot S., Briais A., 2012: Spherical harmonic modeling to ultra-high degree of Bouguer and isostatic anomalies. Journal of Geodesy, **86**, 7, 499–520.

Blakely R. J., 1995: Potential Theory in Gravity and Magnetic Applications: Cambridge, UK, Cambridge University Press, 411 p.

Bonvalot S., Balmino G., Briais A., Kuhn M., Peyrefitte A., Vales N., Biancale R., Gabalda G., Moreaux G., Reinquin F., Sarrailh M., 2012: World Gravity Map, 1:50000000 map, Eds.: BGI-CGMW-CNES-IRD, Paris, CGMW-BGI-CNES-IRD.

Brabant P., 1976: Carte pédologique de reconnaissance, Feuille Rei-Bouba à 1/200000, 107 p. (in French).

Brabant P., Gavaud M., 1985: Les sols et les ressources en Terre du nord-Cameroun. M.E.S.R.E.S., I.R.A., ORSTOM, Not. Exp., **103**, 285 p. (in French). (in French).

Brunet M., Coppens Y., Dejax J., Flynn L., Heintz E., Hell J., 1990: Nouveaux mammifčres du Crétacé inférieur du Cameroun, Afrique de l'Ouest. Comptes Rendus Académie de Sciences, Paris, **310**, II, 1139–1146 (in French).

Brunet M., Jacobs L., Congleton J., Coppens Y., Dejax J., Flynn L., 1988: Première découverte d'un fragment de mandibule de mammifère dans le Crétacé inférieur d'Afrique (Cameroun, bassin de Koum). Comptes Rendus Académie de Sciences, Paris **307**, II, 1675–1680 (in French).

Collignon F., 1968. Gravimétrie et reconnaissance de la République Fédérale du Cameroun ORSTOM Paris, 35 p. (in French).

Duperon-Laudoueneix M., 1991: Les flores ligneuses mésozoïques et cénozoïques d'Afrique nord-équatoriale (Tchad et Cameroun). Thèse doc-d'Etat, Univ. Pièrre et Marie Curie, Paris VI, France, 299 p. (in French).

Kamguia J., Manguelle-Dicoum E., Tabod C. T., Tadjou J. M., 2005: Geological models deduced from gravity data in the Garoua basin, Cameroon. Journal of Geophysics and Engineering, **2**, 2, 147–152.

Maurin J. C., Benkhelil J., Robineau B., 1986: Fault rocks of the Kaltungo lineament, NE Nigeria, and their relationship with Benue trough tectonics. Journal of the Geological Society, **143**, 587–589.

Nolla Junior D., Hell J. V., Ngos Lii S., Bessong M., Mfoumbeng M. P., Eyong Takem J., Dissombo Edimo A. N., Mbang A. R., Engombi Godlove, Ndjeng E., 2015: Lithostratigraphy of the Koum Basin (Northern Cameroon). International Journal of Multidisciplinary Research and Development, **2**, 6, 103–114.

Ogunmola J. K., Ayolabi E. A., Olobaniyi S. B., 2014: Lineament extraction from SPOT 5 and Nigeriasat-x imagery of the upper Benue trough, Nigeria. The International Archives of the Photogrammetry, Remote Sensing and Spatial Information Sciences, Volume XL-1, 2014 ISPRS Technical Commission I Symposium, 17–20, Denver, Colorado, USA.

Ogunmola J. K., Ayolabi E. A, Olobaniyi S. B., 2016: Structural-depth analysis of the Yola Arm of the Upper Benue Trough of Nigeria using high resolution aeromagnetic data. Journal of African Earth Sciences, **124**, 32–43.

Pavlis N. K., Holmes S. A., Kenyon S. C., 2012: The development and evaluation of the Earth gravitational model 2008 (EGM2008). Journal of Geophysical Research, **117**, B04406.

Pirttijärvi M., 2014a: FOURPOT Potential field data processing and analysis of using 2-D Fourier transform, User's guide to version 1.3a: `https://wiki.oulu.fi/display/~mpi/2D+Fourier+domain+operations`.

Pirttijärvi M., 2014b: GRABLOX2 Gravity interpretation and modelling using 3-D block models, user's guide to version 2.1: `https://wiki.oulu.fi/display/~mpi/Gravity+inversion+using+block+model+2`.

Popoff M., 1988: Du Gondwana à l'Atlantique sud; les connexions du fossé de la Benoué avec les bassins du Nord-Est brésilien jusqu'à l'ouverture du golfe de Guinee au Cretace inferieur. Journal of African Earth Sciences, **7**, 2, 409–431.

Schwoerer P., 1965: Carte géologique de reconnaissance à l'échelle du 1/500.000. Notice explicative sur la feuille Garoua Est. Direction des Mines et de la Géologie du Cameroun (éd.), Yaoundé, 49 p. (in French).

Tokam A. P., Tabod C. T., Nyblade A. A., Jordi J., Wiens D. A., Pasyanos M. E., 2010: Structure of the Crust Beneath Cameroon, West Africa, from the Joint Inversion of Rayleigh Wave Group Velocities and Receiver Functions. Geophysical Journal International, **183**, 1061–1076.

Zeng H., 1989: Estimation of the Degree of Polynomial Fitted to Gravity Anomalies and Its Applications. Geophysical Prospecting, **37**, 959–973.

sciendo

Contributions to Geophysics and Geodesy Vol. 48/4, 2018 (299–317)

Refined prediction of vertical gradient of gravity at Etna volcano gravity network (Italy)

Pavol ZAHOREC[1], Juraj PAPČO[2], Peter VAJDA[1], Filippo GRECO[3], Massimo CANTARERO[3], Daniele CARBONE[3]

[1] Division of Geophysics, Earth Science Institute, Slovak Academy of Sciences, Bratislava, Slovak Republic; e-mail: zahorec@savbb.sk

[2] Department of Theoretical Geodesy, Faculty of Civil Engineering, Slovak University of Technology, Bratislava, Slovak Republic

[3] Instituto Nazionale di Geofisica e Vulcanologia, Sezione di Catania, Osservatorio Etneo, Catania, Italy

Abstract: Predicted values of the vertical gradient of gravity (VGG) on benchmarks of Etna's monitoring system, based on calculation of the topographic contribution to the theoretical free-air gradient, are compared with VGG values observed in situ. The verification campaign indicated that improvements are required when predicting the VGGs at such networks. Our work identified the following factors to be resolved: (a) accuracy of the benchmark position; (b) gravitational effect of buildings and roadside walls adjacent to benchmarks; (c) accuracy of the digital elevation model (DEM) in the proximity of benchmarks. Benchmark positions were refined using precise geodetic methods. The gravitational effects of the benchmark-adjacent walls and buildings were modeled and accounted for in the prediction. New high-resolution DEMs were produced in the innermost zone at some benchmarks based on drone-flown photogrammetry to improve the VGG prediction at those benchmarks. The three described refinements in the VGG prediction improved the match between predicted and in situ observed VGGs at the network considerably. The standard deviation of differences between the measured and predicted VGG values decreased from 36 to 13 μGal/m.

Key words: VGG, topographic effect, building correction, DEM, volcano gravity monitoring network

1. Introduction

Many active or dormant volcanoes are monitored by repeated gravity measurements aimed to detect and interpret spatiotemporal gravity changes.

doi: 10.2478/congeo-2018-0014

The latter can be used to study subsurface processes associated with magma dynamics, thus contributing to forecasts about possible eruptive events (e.g. *Battaglia et al., 2008; Carbone et al., 2017; Fernández et al., 2017*). In such time-lapse surveys the knowledge of the true (in-situ) values of the vertical gradient of gravity (VGG) plays an important role. The use of various types of gravity meters, relative and/or absolute that are fitted with sensors at different heights requires proper consideration of the VGG to "reduce" data readings to the ground or to a common level. If the VGG values are not observed in-situ, they can be modeled (predicted). The quality of this prediction is the subject of the presented work, which is focused on a case study from Etna.

The deviation of the in-situ real VGG from the normal (theoretical) value of $-308.6\,\mu$Gal/m ($1\mu\text{Gal/m} = 10^{-8}\text{s}^{-2}$) strongly depends on the nearby topography. A great part of this deviation can be modeled provided that a detailed digital elevation model (DEM) with sufficient resolution (accuracy), as well as correct rock-density information, is available. We have analyzed this topographic contribution to the VGG for the case of Teide volcano on Tenerife, Canary Islands (*Zahorec et al., 2016*). A good agreement was obtained between the calculated (predicted) and the subsequently in-situ verified VGGs on several benchmarks of the Teide gravity monitoring network. These results motivated us to conduct a similar study at Etna volcano.

The gravity monitoring network of Etna (for time-lapse measurements) consists of 71 benchmarks (Fig. 1; *Carbone and Greco, 2007; Greco et al., 2012*). The network is operated by INGV Osservatorio Etneo since 1986 (*Budetta et al., 1989*). Relative gravity surveys have been gradually complemented by 13 absolute gravity points allowing the so-called hybrid microgravity surveys (*Greco et al., 2012*). Several campaigns of VGG measurements have been also realized on absolute as well as relative benchmarks (*Greco et al., 2012; Bonforte et al., 2017*). Our primary effort was to compare the in-situ measured VGGs with our calculated (predicted) values based on the contribution of topographic masses to the gradient. Our first results showed that the match between predicted and observed VGGs was not satisfactory. Therefore, we decided to carry out a dedicated gravity campaign aimed at identifying the causes of the above misfit, at improving the calculation, and at observing some additional in-situ VGG values.

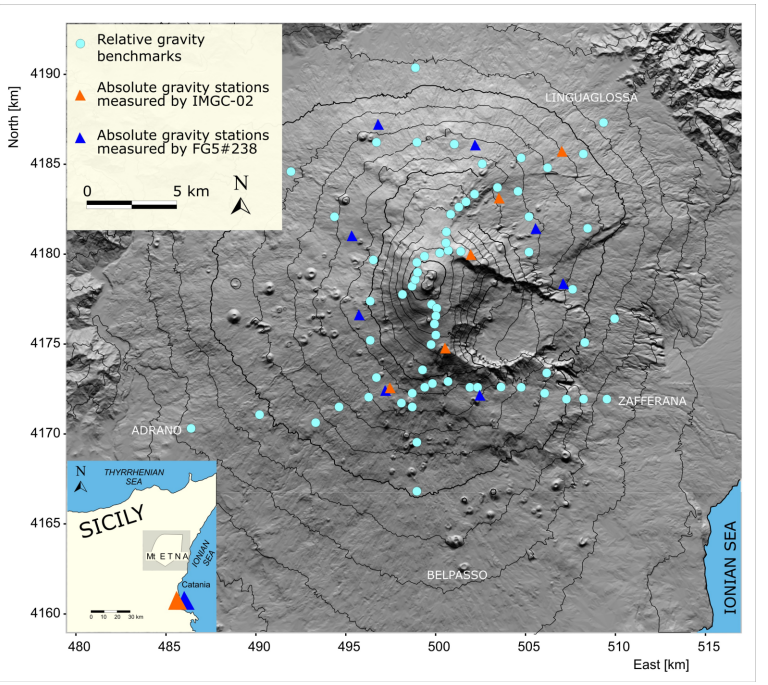

Fig. 1. Sketch map of Etna showing the benchmarks for time-lapse relative (circles) and absolute (triangles) gravity measurements. See upper left inset for explanations.

In the first part of the article we describe the method of the VGG prediction. Next, we focus on in-situ data acquisition and processing and finally we discuss the improvements to the VGG prediction.

2. VGG prediction on the benchmarks of Etna's gravity network

In previous studies (*Vajda et al., 2015; Zahorec et al., 2016*) it was found that in-situ measured VGGs in volcanic areas can deviate significantly from the theoretical value depending on topography conditions (besides the geology contribution which is usually less important in areas of prominent topography). We measured VGG values in the range –125 to –506 μGal/m in the Teide volcano area. Extreme deviations, low and high in absolute sense, are

associated with rough terrain shapes: narrow valleys (gorges, canyons) and sharp convex features (peaks, ridges, caldera rims), respectively.

We predicted the VGG values by computing the topographic (and also bathymetric) contribution to the gradient. To that end, we used the proprietary software Toposk (*Zahorec et al., 2017*). This program was especially developed to calculate the topographic effect (i.e. the gravitational effect of the masses between the topo-surface and the zero level) at arbitrary point locations, e.g. above or below the topographic surface. This comes very handy when VGGs are calculated over benchmarks that lie below the terrain level. Such is the case of the absolute point at the Pizzi Deneri volcanological observatory (PDN; 2820 m a.s.l.), located in the basement of the observatory.

The topographic contribution to the VGG is simply computed as the difference between the topographic effects calculated at the heights of 1.25 and 0.25 m, respectively, above the surface. These heights equal approximately to the CG-5 gravity meter sensor positions during the VGG measurements in the field using a tower. The topographic (and also bathymetric) effect is considered up to the standard distance of 166.7 km, while the integration area is divided into the following zones: inner zone up to 250 m around the calculation point, intermediate zone 250–5240 m and outer zones from 5.24 up to 166.7 km. The inner and intermediate zones play dominant roles in the contribution to the VGG. A high-precision DEM, such as those derived from LiDAR data, is required especially within the inner zone. In the presented study we used an available LiDAR-based DEM produced by *Bisson et al. (2015)*. The DEM was produced by INGV (Sezione di Pisa), on the grounds of a survey completed in 2005. The original DEM with spatial resolution of 2 m (vertical accuracy of ± 0.24 m) was resampled to 5 m resolution (provided in ASCII format). Final grid was computed using the Surfer software using Nearest Neighbor interpolation procedure with the grid cell size of 5 m (Fig. 2). Although this DEM is of relatively high quality, it does not account for morphological changes that occurred in some areas after 2005. In addition, some parts of the model feature a lower quality (due to missing LiDAR data). These facts complicate our VGG prediction. Therefore, we decided to complement the DEM through detailed drone-flown photogrammetry models in the nearest zone, wherever necessary and possible.

The topographic as well as bathymetric contributions from the outer

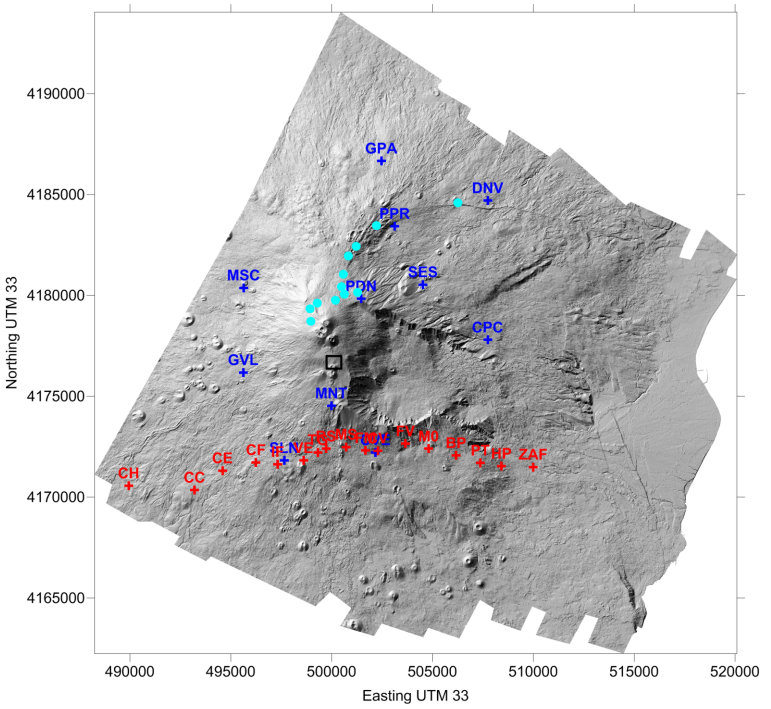

Fig. 2. Shaded relief map of the LiDAR-based DEM (*Bisson et al., 2015*) with the positions of measured and predicted VGG points. Absolute gravity points are blue crosses, relative benchmarks are red crosses. Cyan circles represent points along the NE-rift. The little black square encloses the cloud of points with observed VGGs near the Torre del Filosofo area (2800 m a.s.l.).

zones (beyond 5.24 km) were calculated using SRTM data (*Jarvis et al., 2008; Olson et al., 2016*). The maximum topographic contribution to the VGG from the outer zones represents about +20 μGal/m (10^{-8}s^{-2}). For comparison, the maximum contribution from the inner and intermediate zones is –176 μGal/m (for the density of 2670 kg/m^3). The bathymetric contribution to the VGG (for the density of –1640 kg/m^3) in our Etna area is negligible, it amounts to only –1 to –2 μGal/m.

The correct estimation of the density of topographic masses can be a serious problem due to high rock-density variability in volcanic areas. For example, in the case of Teide volcano the adopted density of 2200 kg/m^3 yielded in general successful results (*Zahorec et al., 2016*), but with caution

that the real density could be even considerably smaller in some places such as the areas of young slag lavas or thermally altered layers. As Etna represents a large basaltic composite volcano (*Branca et al., 2011*), we opted for a higher density. We have used the density of 2670 kg/m^3, which is in accordance with *Schiavone and Loddo (2007)*, who used this value as reference density for the Bouguer anomaly map of Etna.

The total (from all integration zones) estimated topographic contribution to the VGG is added to the theoretical value –308.6 μGal/m to predict the VGG at a given point. Figure 3 shows the predicted VGG values compared with the measured ones on absolute gravity points and relative benchmarks.

Figure 3 shows that the fit between measured and predicted values is generally not good (notice that some measured VGGs are scattered due to poor

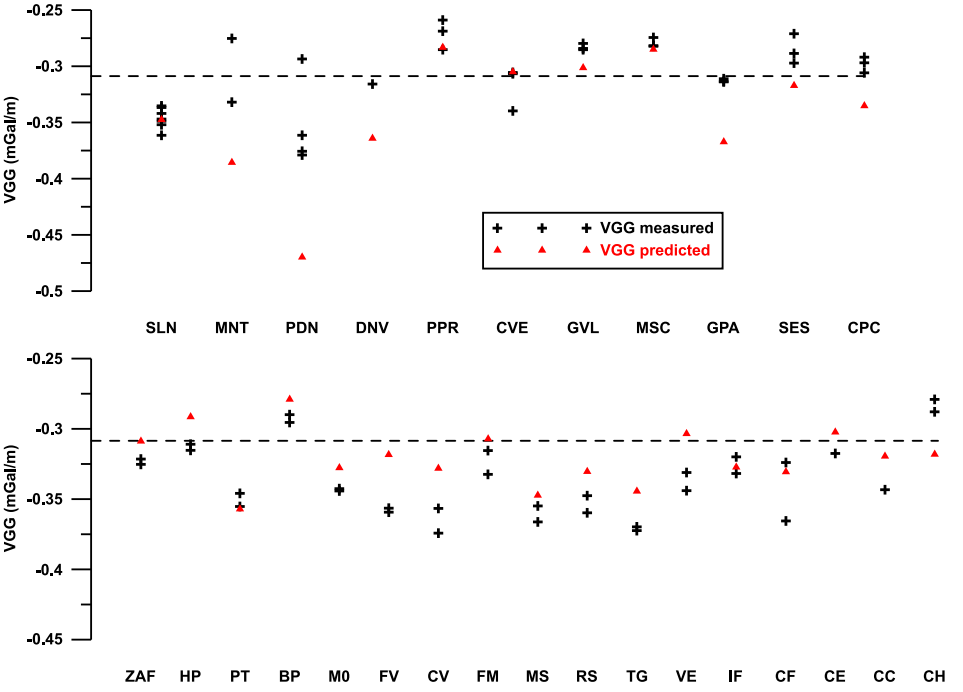

Fig. 3. Predicted VGGs (red triangles) on absolute gravity points (upper graph) and relative benchmarks (bottom graph). Black crosses represent measured VGGs. Dashed line represents theoretical (normal) VGG of –308.6 μGal/m. Station positions are shown in Fig. 2.

observation conditions). The first cause of misfit we considered was a possible station position error. We assumed this error because we knew that the stations were not positioned using precise geodetic point positioning (point coordinates were determined only by hand-held GPS). In addition, there seemed to be a systematic shift between measured and predicted VGGs. In the case of absolute gravity points a systematic shift to higher predicted values (in their absolute value) was apparent, while relative points exhibited an opposite tendency (Fig. 3). On the ground of previous observations, we hypothesized that this could be due to local positioning and near building effects (*Zahorec et al., 2014*). Therefore, we decided to perform additional in-situ observations, aimed at (i) verifying the position of the observation points and (ii) precisely determining the geometrical characteristics of anthropic structures (walls, buildings, etc.) in close vicinity to relative and absolute gravity points, in order to model their effect on VGG values.

We also planned to verify the VGGs measured in 2009 (*Maucourant et al., 2014*) along a cloud of points clustered in a small area near the 2002 eruptive vent (see little square in Fig. 2). We realized that our prediction at these points was completely inadequate (Fig. 4). Indeed the topography of this area underwent a drastic change, due to the fall-out products erupted from Etna's main craters. We mention this to illustrate that on active volcanoes large topographic changes may occur over relatively short intervals, implying that the available DEM may become inadequate in some parts shortly after its production.

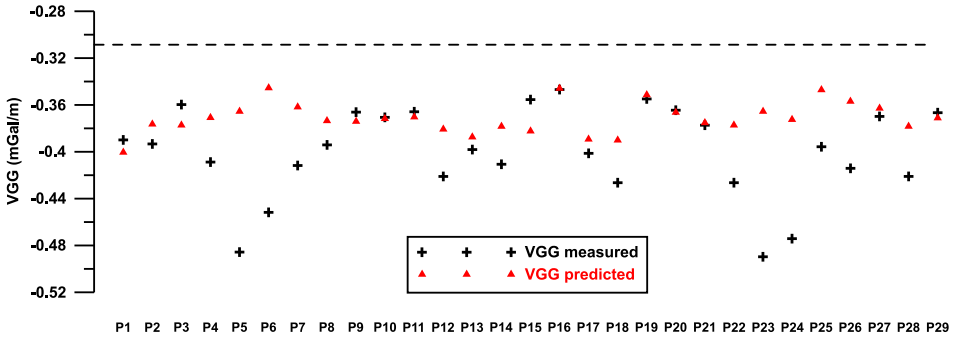

Fig. 4. Misfit between predicted (red triangles) and measured (black crosses) VGGs at Torre del Filosofo area in 2009. Dashed line represents theoretical (normal) VGG of –308.6 μGal/m.

We focused also on benchmarks of the gravity-deformation monitoring profile established in the area of the NE-rift (Fig. 2). The measurements between 2002 and 2003 captured very high vertical displacements (more than 2 m) associated with the 2002–2003 NE-rift eruption, as well as gravity variations up to 350 μGal already corrected for the free-air effect using the normal free-air gradient –308.6 μGal/m (*Bonforte et al., 2007*). At the benchmarks of this profile the true VGG values were not known. We thus decided to assess the difference between the free-air correction based on predicted and theoretical VGGs. Since our prediction indicated VGG values quite different from normal free-air gradient on several benchmarks, a successful prediction would be of great value, particularly in this case, where a large difference between gradients is multiplied by a very large vertical displacement, see Table 1. Due to harsh observation conditions (strong wind in combination with unstable ground) in-situ measurements could be performed at only one of the NE-rift benchmarks, see next chapter.

Table 1. Expected deviation in free-air correction as a result of difference between predicted VGG and normal free-air gradient (-308.6μGal/m) multiplied by observed vertical displacement at three selected benchmarks of the NE-rift gravity-deformation monitoring profile (cyan circles in Fig. 2).

Point	Vertical displacement (m)	Predicted VGG (μGal/m)	Expected deviation (μGal)
LZ	–2.16	–371	135
DG	–2.329	–357	113
CO	–1.403	–374	92

3. In-situ geodetic and VGG observations

In July 2018 we conducted a gravity campaign on Etna in order to make precise in-situ geodetic positioning on microgravity network points as well as to verify several VGG predictions. Our goal was to improve consistency between calculated (predicted) and in-situ measured VGGs on network benchmarks. In addition, we also carried out new VGG measurements with the same objective.

Spatial coordinates of all benchmarks, as well as of ground control points (GCP) for our surveying and photogrammetry, were determined using GNSS

and traditional terrestrial measurements. GNSS measurements used Network and Satellite based Real Time Kinematic (NRTK/SRTK) or Fast Static Post-processing (FS) mode. NRTK measurements were realized using the Italy HEXAGON positioning service HxGN SmartNet (`http://it-xpos.nrtk.eu/spiderweb/frmIndex.aspx`) in Virtual Reference Station concept. SRTK measurements were realized using satellite Trimble RTX technology (`https://www.trimble.com/positioning-services/trimble-rtx.aspx`).

SRTK and Fast static method with precise post-processing was used on sites with no internet connection or with bad observation conditions (near the trees). For FS method the nearest permanent GNSS stations from Etna's geodetic network (*Palano et al., 2010*) or HxGN SmartNet GNSS network were used as reference points. Traditional terrestrial measurements were performed in the places without GNSS signal availability (in the buildings or in the forests). Measurements were realized with the Trimble R10 GNSS receiver and Trimble M3 total station. Average observation period was about 3 minutes in the case of the NRTK measurements, and about 20–30 minutes in the case of the SRTK or fast static measurements. Final processing was performed in Trimble Business Centre (v. 4.10) software. Spatial positions of the points were determined primarily in the ETRS89 coordinates system and then transformed to UTM33 projection. Physical heights of the points were transformed from ellipsoidal ones using global geopotential model EGM2008 (*Pavlis et al., 2012*). Horizontal and vertical accuracy achieved for the VGG and GCP points is better than 5 cm.

After processing the measurements we found differences between new exact GNNS coordinates and the previous approximate positions to be in the range of 0.7 to 28 m in horizontal position and 0.4 to 10 m in vertical position.

The majority of relative benchmarks is situated on the roadside rockwalls (Fig. 5). This is for practical reasons: during the winter season the benchmarks do not get covered by the snow piled up by snow plows. The gravity effect on the gradient of these walls is not negligible, and thus it has to be modeled. Therefore we precisely measured the dimensions of the walls as well as benchmark positions with respect to the walls, and calculated their effect that was added to the nearest zone contribution in VGG prediction.

Fig. 5. GNNS measurements on one of relative benchmarks situated on the top of roadside rock-wall (top) and in the front of a refuge with an absolute gravity point inside (bottom).

The absolute gravity points are typically situated inside accessible small refuges (see an example in Fig. 5), except PDN and MNT. PDN is situated inside the basement of the Pizzi Deneri volcanological observatory (managed by INGV Catania). This point is actually underground, which caused the worst VGG prediction (see Fig. 3). MNT is situated inside the build-

ing of the upper cable-car station. However, this point was not accessible during our campaign. At all absolute gravity points we took the GNSS measurement at an open-air place in their proximity from which we positioned the gravity benchmark inside a building using terrestrial measurements by means of total station. We also measured the dimensions of the buildings and the thickness of their walls, as well as the relative position of benchmark with respect to the building walls (using laser rangefinder), in order to be able to carry out subsequent building correction calculation.

In addition to GNSS/terrestrial geodetic measurements, we also aimed at improving the topographic effect calculation in the nearest zone using drone-flown photogrammetry wherever feasible and applicable. Aerial images were taken in the surrounding of the selected absolute/relative benchmarks (diameter of 50 to 120 m around the point) using the unmanned aerial vehicle – DJI Phantom v. 3 and 4. Minimum six artificial GCPs were prepared and distributed before the flight at each locality. Checked and cleaned stereoscopic images with at least 60% longitudinal and latitudinal overlap were processed using Agisoft PhotoScan (`http://www.agisoft.com/`) with standard processing chain into classified point clouds, digital elevation models and georeferenced orthophotomosaics. The quality of the photogrammetric processing was checked using GCPs and independent sets of points and varies between 3–7 cm in the horizontal position and 5–13 cm in the height. The automatic classification to the ground class was improved by supervised selection of individual trees, buildings or artefacts (see Fig. 7) in Surfer v. 15. Final digital terrain/surface models with the resolution of 0.5 m were created in Surfer v. 15 using Kriging interpolation method.

Because of inappropriate environmental conditions (presence of trees, strong wind preventing the drone flight) we managed to perform drone-borne photogrammetry only at five benchmarks (see Fig. 2): TG, CV, PDN, GVL and the new point MNT_IG, where the iGrav# 020 superconducting gravity meter was installed by INGV team in 2016.

We repeated VGG measurements on benchmarks CF and DNV to confirm older measurements (Fig. 3). We made new VGG measurements at two points, LZ and MNT_IG. The VGG measurements were performed in a tower mode using relative gravity meter CG-5 and geodetic tripod (Fig. 6). Gravity acceleration at each point was measured by A-B-A-B-A repeating method at two height levels (with gravity meter sensor approximately 0.25m

Fig. 6. Tower VGG measurement at point LZ (in its top position) in unusual conditions (with a view of NE creater in the background). Umbrella had to be used to shield the meter from wind.

(A) and 1.3m above the ground (B), depending on the tripod setup). The exact height of the gravity meter sensor above the ground (point/benchmark) was measured using the smart high-precision laser distance meter. Striking wind posed a serious problem for the tower VGG measurement accuracy at several points, especially in the upper measuring position (B) on the tripod. We used a common umbrella (Fig. 6) to shield the gravity meter from the wind, but it was very problematic to get reasonable results in several cases. The strong wind was the reason why we were able to get the VGG at only one of three scheduled points in the NE-rift area. We have estimated a measurement error at particular measurement levels (A and B) of approximately $\pm 7\,\mu$Gal, which leads to an error of about $\pm 10\,\mu$Gal/m in VGG.

At the new point MNT_IG, which is situated at the Montagnola hut on the top of an extinct crater (2600 m a.s.l.), we acquired the highest (in absolute sense) VGG value of –454 μGal/m, which represents a deviation of 47% from the normal gradient. For a comparison, *Greco et al. (2012)* reported previously measured gradients on Etna network benchmarks with deviations of up to about 25%.

4. Near topography refinement and building corrections

All in-situ determined data, i.e. accurate horizontal positions and elevations of benchmarks and new measured VGG points (with exact gravity meter sensor heights above the ground), building and roadside wall dimensions, as well as drone-borne photogrammetry-derived DEMs of the nearest zones, were subsequently used to improve the VGG calculation (prediction).

Topographic contribution to the VGG was calculated in the same manner as described previously, using the density of 2670 kg/m^3. Real heights of the gravity meter sensor with respect to the ground were kept in this case. Using exact coordinates and heights of the benchmarks yields an improvement of the topographic contribution in the range from –45 to +23 μGal/m (standard deviation of 15 μGal/m), while the topographic contributions to the VGG itself ranges from –165 to +93 μGal/m. The highest negative contribution is at point MNT_IG situated on the top of an extinct crater, the highest positive contribution is at point PDN situated in underground setting. In addition, drone-borne photogrammetric DEMs of the nearest zone were used to improve the innermost zone contribution at five points (within the distance of up to approximately 80 m). This improvement is less than 10 μGal/m at all points except for point PDN, where it reaches 52 μGal/m due to the fact that the point is located in the basement of the observatory (Fig. 7).

The gravitational effect of building walls, roadside walls, as well as concrete pillar was modeled by means of simple rectangular prisms using the software Potent (*Potent, 2010*). The real position of the gravity meter sensor with respect to the modeled bodies was accounted for, based on the in-situ measured distances using laser rangefinder. While the geometric definition of the modeled prisms is simple, the estimation of their density is still problematic. We took into account the brick material (basalt) as well as its porosity, so we chose the density of 2500 kg/m^3 for compact walls and 2200 kg/m^3 for the walls made of rocks with higher porosity. In case of the concrete pillar (protruding above floor level) we used the density of 2300 kg/m^3. Station PDN required special attention as it is situated underground. After the calculation of topographic effect (using drone-borne photogrammetric DEM in the innermost zone, see Fig. 7) for a true underground position of the point, we had to also model "empty" underground

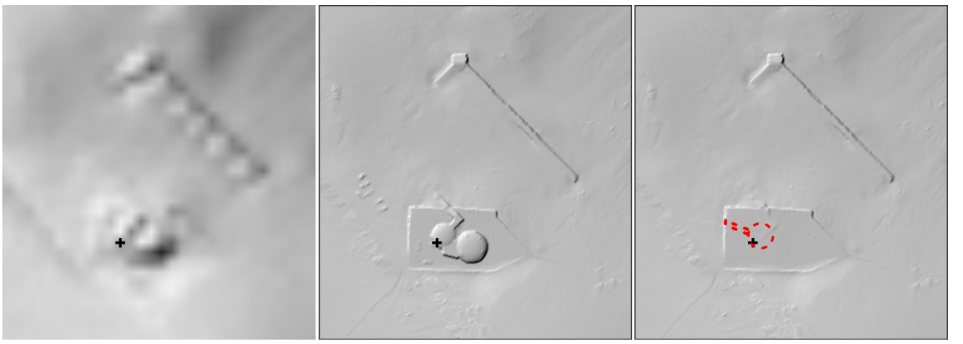

Fig. 7. Comparison of the LiDAR-based DEM (left) with the drone-borne photogrammetric DEM (middle) in the vicinity of the absolute gravity point PDN (black cross) situated in the basement of Pizzi Deneri volcanological observatory (2820 m a.s.l.). The right picture shows the "cleaned" model that was used for the topographic effect calculation. Red dashed line indicates the position of underground basement, which was subsequently also modeled (see Fig. 8).

spaces, see Fig. 8.

Thus calculated building contributions to the VGG reach –5 to –15 μGal/m in case of relative benchmarks situated on roadside walls, and +14 to +26 μGal/m in case of absolute gravity points located inside buildings (note that opposite sign of these contributions corresponds to the opposite systematic "shifts" observed from prediction, see Fig. 3). A special case is again PDN, where the "basement" contribution (see Fig. 8) reaches –140 μGal/m, but this contribution and the topography contribution compensate

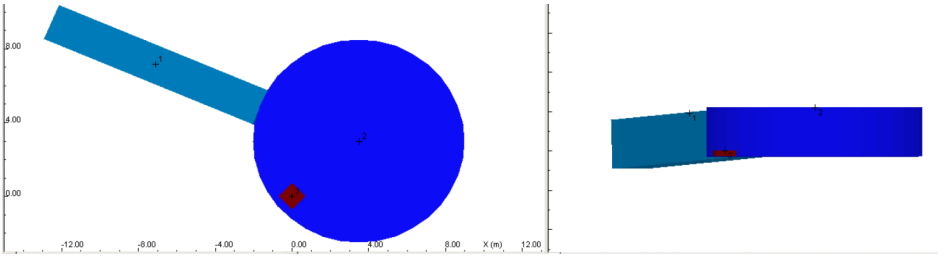

Fig. 8. Modeled underground spaces around point PDN (left – top view, right – side view). Blue model bodies represent basement room with inclined access corridor, small red prism represents a concrete pillar protruding above the floor level. Picture is taken from Potent modeling software interface, axis units are in meters.

each other to a significant extent.

Since the points GPA and ZAF are located near local terrain steps with a height of approximately two meters, which are not adequately captured by the LiDAR DEM, we used simple prism approximation of these edges to estimate their contribution to the VGG. We estimated these contributions to be +17 and –8 μGal/m for GPA and ZAF, respectively (note that opposite sign of these contributions corresponds to opposite field conditions, GPA lies below the terrain edge while ZAF lies on the top of the edge).

Fig. 9 shows comparison between measured VGGs and VGG values calculated (i) using previously available information and (ii) the new information described above (in case of repeated VGG measurements at the same benchmark the portrayed VGG value represents the average values).

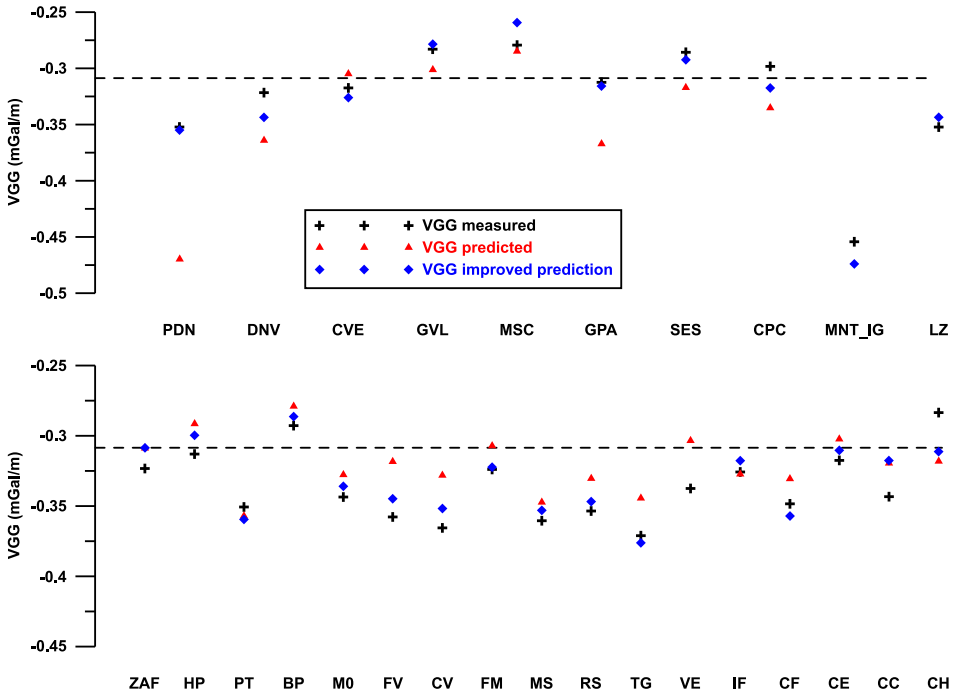

Fig. 9. Comparison of averaged measured VGGs (black crosses) with previously predicted VGGs (red triangles, also shown in Fig. 3) and newly calculated values (blue diamonds) on absolute gravity points (upper graph) and relative benchmarks (bottom graph). Dashed lines represent theoretical (normal) gradient of –308.6 μGal/m.

5. Discussion

A relatively good improvement of newly calculated VGGs was achieved in comparison with previously predicted values at most benchmarks (demonstrated by the shift of blue marks closer to the black ones in Fig. 9). Regarding the absolute gravity points (Fig. 9, upper graph), there is a shift towards positive VGG values in most cases, which is mainly the result of introducing the building correction. The most significant improvement has been achieved at PDN, after including the correction for the underground positioning of the gravimeter.

Two newly measured VGG points MNT_IG and LZ are also shown in the mentioned graph. They show a good correlation between measured and calculated VGG values, as they are located outdoor (see Fig. 6), implying that the correction accounting for the hosting building is not needed. At LZ, the difference between the in-situ measured (–352 μGal/m) and the theoretical (–308.6 μGal/m) VGG can lead to a significant difference in the free-air correction if large vertical displacements (> 2 m) occur, as in the case of the ground deformation associated with the 2002–2003 NE-rift eruption (*Bonforte et al., 2007*), cf. Table 1.

Relative benchmarks show an opposite behavior (Fig. 9, bottom graph), as they exhibit a shift towards negative VGG values in most cases. This results from the improved topographic correction, as well as the roadside wall corrections. The correlation between measured and newly calculated VGG values is significantly better at most points compared with previously predicted values, but there are still some points where predictions are not satisfactory, especially points CC, CH. These points are situated under trees, so it was not possible to perform drone photogrammetry and get more accurate terrain models.

6. Conclusions

We can statistically evaluate the improvement of the VGG prediction as follows: standard deviation of differences between measured and predicted VGG values decreased from 39 to 13 μGal/m at absolute gravity points and from 18 to 12 μGal/m in case of relative benchmarks. In terms of maximum

differences (in absolute sense) we got improvement from 117 to 22 μGal/m (absolute points) and from 39 to 28 μGal/m (relative points). Regarding the relative importance of the different contributions to VGGs, we have to distinguish between "surface" benchmarks and the underground PDN point. At PDN, an important contribution to VGG comes from considering the empty underground spaces. Furthermore, drone-borne photogrammetry allowed to improve the topographic contribution of the inner-zone (a difference of 52 μGal/m was found for this component). Conversely, the inner-zone topographic contribution improvement was relatively small at other points (less than 10 μGal/m). In the case of absolute gravity points, the correction accounting for the building that hosts the gravimeter reaches 26 μGal/m in maximum. Finally, the accurate geodetic re-positioning of benchmarks resulted in an improvement in the topographic contribution of up to 45 μGal/m. These results indicate that accurate VGG predictions require precise information on topography and point positioning, as well as consideration of the contribution from man-made structures in close proximity to the observation point.

Acknowledgements. This work was supported by the VEGA grant agency under projects No. 2/0042/15 and 1/0462/16 as well as by the Slovak Research and Development Agency, grant No. APVV-16-0482 (acronym Lithores).

References

Battaglia M., Gottsmann J., Carbone D., Fernández J., 2008: 4D volcano gravimetry. Geophysics **73**, 6, WA3–WA18, doi: 10.1190/1.2977792.

Bisson M., Spinetti C., Neri M., Bonforte A., 2015: Mt. Etna volcano high-resolution topography: airborne LiDAR modelling validated by GPS data. International Journal of Digital Earth, doi: 10.1080/17538947.2015.1119208.

Bonforte A., Carbone D., Greco F., Palano M., 2007: Intrusive mechanism of the 2002 NE-rift eruption at Mt. Etna (Italy) modelled using GPS and gravity data. Geophys. J. Int., **169**, 339–347, doi: 10.1111/j.1365-246X.2006.03249.x.

Bonforte A., Fanizza G., Greco F., Matera A., Sulpizio R., 2017: Long-term dynamics across a volcanic rift: 21 years of microgravity and GPS observations on the southern flank of Mt. Etna volcano. J. Volcanol. Geotherm. Res., **344**, 174–184.

Branca S., Coltelli M., Groppelli G., Lentini F., 2011: Geological map of Etna volcano, 1:50,000 scale. Ital. J. Geosci. (Boll. Soc. Geol. It.), **130**, 3, 265–291, doi: 10.3301/IJG.2011.15.

Budetta G., Grimaldi M., Luongo G., 1989: Variazioni di gravit'a nell'area etnea (1986–1989). Boll. GNV, **5**, 137–146 (in Italian).

Carbone D., Greco F., 2007: Review of Microgravity Observations at Mt. Etna: A powerful Tool to Monitor and Study Active Volcanos. Pure Appl. Geophys., **164**, 769–790, doi: 10.1007/s00024-007-0194-7.

Carbone D., Poland M. P., Diament M., Greco F., 2017: The added value of time-variable microgravimetry to the understanding of how volcanoes work. Earth-Science Reviews **169**, 146–179, doi: 10.1016/j.earscirev.2017.04.014.

Fernández J., Pepe A., Poland M. P., Sigmundsson F., 2017: Volcano Geodesy: Recent developments and future challenges. J. Volcanol. Geotherm. Res., **344**, 1–12.

Greco F., Currenti G., D'Agostino G., Germak A., Napoli R., Pistorio A., Del Negro C., 2012: Combining relative and absolute gravity measurements to enhance volcano monitoring. Bull. Volcanol., **74**, 1745–1756.

Jarvis A., Reuter H. I., Nelson A., Guevara E., 2008: Hole-filled SRTM for the globe Version 4, available from the CGIAR-CSI SRTM 90m Database: http://srtm.csi.cgiar.org.

Maucourant S., Giammanco S., Greco F., Dorizon S., Del Negro C., 2014: Geophysical and geochemical methods applied to investigate fissures-related hydrothermal systems on the summit area of Mt. Etna volcano. J. Volcanol. Geotherm. Res., **280**, 111–125, doi: 10.1016/j.jvolgeores.2014.05.014.

Olson Ch. J., Becker J. J., Sandwell D. T., 2016: SRTM15_PLUS: Data fusion of Shuttle Radar Topography Mission (SRTM) land topography with measured and estimated seafloor topography (NCEI Accession 0150537). Version 1.1. NOAA National Centers for Environmental Information.

Palano M., Rossi M., Cannavò F., Bruno V., Aloisi M., Pellegrino D., Pulvirenti M., Siligato G., Matiia M., 2010: Etn@ref: a geodetic reference frame for Mt. Etna GPS networks. Annals of Geophysics, **53**, 4, doi: 10.4401/ag-4879.

Pavlis N. K., Holmes S. A., Kenyon S. C., Factor J. K., 2012: The development and evaluation of the Earth Gravitational Model 2008 (EGM2008). Journal of Geophysical Research: Solid Earth, **117**, B04406: http://dx.doi.org/10.1029/2011JB008916.

Potent v.4.11.06, 2010: User guide. Manuscript, Geophysical Software Solutions Pty. Ltd., Gungahlin, Australia.

Schiavone D., Loddo M., 2007: 3-D density model of Mt. Etna Volcano (Southern Italy). Journal of Volcanology and Geothermal Research, **164**, 161–175.

Vajda P., Zahorec P., Papčo J., Kubová A., 2015: Deformation induced topographic effects in inversion of temporal gravity changes. Contributions to Geophysics and Geodesy, **45**, 2, 149–171.

Zahorec P., Papčo J., Mikolaj M., Pašteka R., Szalaiová V., 2014: The role of near topography and building effects in vertical gravity gradients approximation. First Break,**32**, 1, 65–71.

Zahorec P., Vajda P., Papčo J., Sainz-Maza S., Pereda de Pablo J., 2016: Prediction of vertical gradient of gravity and its significanse for volcano monitoring – example from Teide volcano. Contributions to Geophysics and Geodesy, **46**, 3, 203–220.

Zahorec P., Marušiak I., Mikuška J., Pašteka R., Papčo J., 2017: Numerical Calculation of Terrain Correction Within the Boguer Anomaly Evaluation (Program Toposk), chapter 5, 79–92, In book: Roman Pašteka, Ján Mikuška and Bruno Meurers (Eds.): Understanding the Bouguer Anomaly: A Gravimetry Puzzle, Elsevier, ISBN 978-0-12-812913-5, doi: 10.1016/B978-0-12-812913-5.00006-3.

sciendo

Contributions to Geophysics and Geodesy Vol. 48/4, 2018 (319–336)

Estimation of Bouguer correction density based on underground and surface gravity measurements and precise modelling of topographic effects – two case studies from Slovakia

Pavol ZAHOREC[1], Juraj PAPČO[2]

[1] Division of Geophysics, Earth Science Institute, Slovak Academy of Sciences, Banská Bystrica, Slovak Republic; e-mail: zahorec@savbb.sk

[2] Department of Theoretical Geodesy, Faculty of Civil Engineering, Slovak University of Technology, Bratislava, Slovak Republic

Abstract: We present a simple and straightforward method for estimating the mean density of topographic masses based on underground gravity measurements along with topography modelling. Two examples under different conditions are given, the first coming from a railway tunnel passing through a Mesozoic karst area and the second from an active coal mine situated in a Neogene sedimentary basin. Relative gravity measurements were processed and corrected by topographic effect modelling based on high-precision airborne LiDAR-derived elevation models. In addition, detailed mining tunnel gravimetric modelling based on terrestrial laser scanning data is presented. Resulted mean (bulk) densities are compared with those obtained from detailed surface gravity measurements as well as with available rock-samples density analysis.

Key words: Bouguer correction density, underground gravity, topographic effect, digital elevation model

1. Introduction

Calculation of Bouguer anomaly requires proper correction (reduction) density estimation. While the density of 2.67 g/cm^3 (1 g/cm^3 = 10^3 kg/m^3) is generally used in global or regional studies (e.g. *LaFehr, 1991; Hinze et al., 2005*), in local studies the correction density should represent a real topographic rock density within the given area. The Bouguer correction density is often estimated directly from the surface gravity measurements by simple

doi: 10.2478/congeo-2018-0015

correlation of Bouguer anomalies with topography (*Nettleton, 1939*). More straightforward comparing of near topographic effect with free-air anomalies in the territory of Slovakia was recently studied in *Mikuška et al. (2014, 2017)*.

The utility of underground gravity measurements for the density determination is well known. The gravity difference between a station at the surface and a vertically offset underground station depends on the mean density of the Earth, as well as on the density of the rock layer between the stations (e.g. *Domzalski, 1955*). Knowing one of these densities the other one can be determined, while the determination of the average rock layer density is generally more reliable.

In this paper we deal with gravity measurements using standard relative gravity meters, performed at the surface and in underground mines, shafts, tunnels etc. However there is a close connection with borehole gravity surveys. As *Hammer (1950)* wrote, his survey with standard-type gravimeter in vertical shaft was made to simulate the data, which would be obtained by a borehole gravimeter.

There is a reason why we could consider the density determination by underground gravity measurements as superior to other methods. As *Hammer (1950)* and *Domzalski (1955)* mentioned, the average (integrated) bulk density of the rocks is exactly what we need in gravity prospecting. In addition, such density can generally differ from the densities obtained from the measurements on rock samples.

Pícha (1953) published results of gravity measurements along the vertical shaft in the mine "Anna" near Příbram in the present-day Czech Republic. And later there were other underground gravity works in the Czech Republic including experimental gravity and vertical gravity gradient measurements in the mine shaft Stonava on which we collaborated (*Pospíšil et al., 2013*). Within the territory of the present-day Slovak Republic, however, so far we have knowledge only about unpublished pioneering underground gravity measurements in mining workings of Maar in *Vybíral et al. (1990)*. The absence of modern underground gravity works in our country also motivated us to perform such measurements.

The issue of rock-densities in the territory of Slovakia is currently under consideration in *Šamajová and Hók (2018)*. The authors summarized the already published density information (coming mainly from rock-samples

analysis) and they subsequently attempted to assign a characteristic density interval to the main geologic/tectonic units present in Slovakia. As they realized, there is a very high variability of the rock densities, both laterally and vertically. Therefore, the question of proper density determination for local gravity surveys is still an open issue. In this article we present a method that enables to determine Bouguer correction density in-situ.

Currently, the LiDAR technique is often used for the generation of high-resolution digital elevation models (DEM) with their wide applicability in various areas. We successfully used the LiDAR data for the vertical gravity gradient prediction (*Zahorec et al., 2016*), where the exact calculation of the near topographic effect is crucial. The use of terrestrial laser scanning for the near terrain correction calculation is described by *Schiavone et al. (2009)*. Here we have used LiDAR-based elevation models, as well as terrestrial laser scan models for the precise near-zone topographic effect calculations presented in this paper.

In the first part of the article we describe the methodology for density determination. Then, two case studies are presented.

2. Methods of rock density determination from underground gravity measurements

The classical approach to determine mean rock density from underground gravity measurements (e.g. *Hammer, 1950*) is based on the following relation for gravity change along the vertical underground depth interval ΔH:

$$\Delta g = (F - 4\pi\kappa\sigma)\Delta H + \Delta T, \tag{1}$$

where F is the free-air vertical gradient (–0.3086 mGal/m), κ is the gravitational constant, σ is the density and ΔT represents the variation of the terrain correction over the elevation interval ΔH. The right-hand side of Eq. 1 (except of the term ΔT) is also called Poincaré-Prey reduction. By inserting the known values the desired density can be expressed from Eq. 1 as follows:

$$\sigma = 3.683 - 11.933\,\Delta g/\Delta H, \tag{2}$$

assuming that Δg is corrected for topography undulations, as well as for underground excavations (shaft, mine, tunnel, etc.). The density calculated using Eq. 2 is expressed in g/cm^3, while the gravity is in mGal and the elevation in m. Introduction of the terrain (and excavations) correction into Eq. 2 requires input density estimation. As *Hammer (1950)* writes, this term is so small that no appreciable error is introduced by using an assumed value of the density for it. However, it is still a source of a potential additional error. A method presented below overcomes this complication.

Another source of potential error in density determination arises from anomalous vertical gradients associated to local or regional gravity anomalies. The presence of anomalous bodies can be estimated from Bouguer anomaly maps or from additional gravity measurements (*Hammer, 1950*). Because of the known geological situation in our study areas, we do not expect local anomalous bodies, which could potentially cause anomalous vertical gradients.

Unlike the classical method, the presented approach is simpler and more straightforward. After correcting the measured gravity difference between the vertically separated surface and underground gravity stations using the normal VGG (again, presuming there is no abnormal VGG caused by anomalous sources), we can assign the resultant gravity difference Δg (which in fact equals to the difference in the free-air anomalies) to the difference in the effect of the topography (meaning the gravitational effect of the masses between the topo-surface and the zero level, the so-called Near Topographic Effect – NTE), taking into consideration the effect of the underground objects (tunnel, mine). Therefore the density value can be simply obtained by dividing the Δg by the ΔNTE, while NTE is calculated for the density of +1.0 g/cm^3 and the tunnel/mine effect for the density of –1.0 g/cm^3. It should be noted that the situation is a little complicated if the measuring points lie below seal level, we will discuss this briefly later.

The NTE is calculated using the proprietary software Toposk (*Zahorec et al., 2017a*). The program enables to calculate very precise topographic effect at arbitrary point location, e.g. above or below the topographic surface, the latter being a special case of underground gravity stations. The NTE is considered up to the standard distance of 166.7 km, while the calculated area is divided into the following zones: inner zone up to 250 m from the calculation point, intermediate zone 250–5240 m and outer zones from 5.24

up to 166.7 km. The inner and intermediate zones play dominant roles, so they must be considered more carefully. We have used high-precision DEMs derived from LiDAR data within the inner zone.

The effects of underground objects (tunnel, mine) were calculated using two approaches. First we tried to use again the Toposk software and DEMs prepared from terrestrial laser scanning data. As the Toposk program requires input elevation models in grid format, the excavated object must be defined using two complementary grids. The effect of the object is calculated simply as a difference between the topographic effects of the top and the bottom topo-surface (grid), see an example in Fig. 1. We have successfully used this approach in the case of railway tunnel (case study I), as we had a detailed laser scan model available over the whole tunnel (performed by Amberg Tunnel Scan system). On the other hand, as we did not have such model available from the mine (case study II), we tried to perform laser scanning using the total station Trimble SX10. But as we have realized, this task has become very difficult due to the presence of a dense fog inside the mine. Therefore we were not able to model the mining corridor up to a sufficient distance around all measurement stations employing laser scan data. Thus we utilized Potent software (*Potent, 2010*) for modelling using a polygonal prism approach, while the cross section of the mining corridor was taken from the closest laser scan data (Fig. 2) or from hand-held laser distance meter measurements.

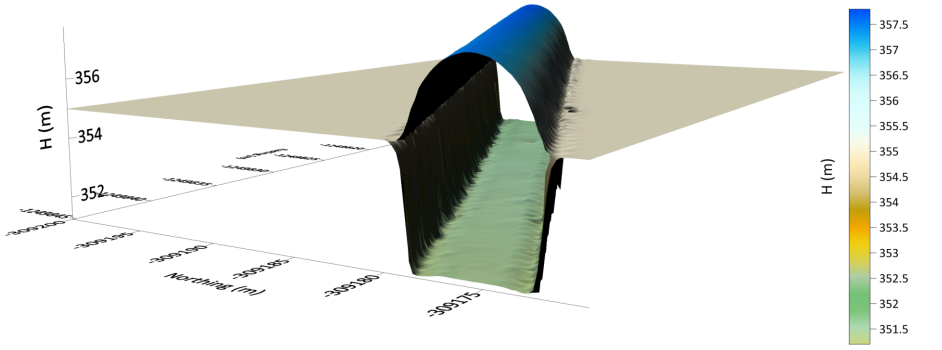

Fig. 1. An example of underground object (tunnel) modelled by two topo-grids. Gravitational effect of the tunnel is calculated using Toposk software simply as a difference between topographic effects defined by particular topo-surfaces.

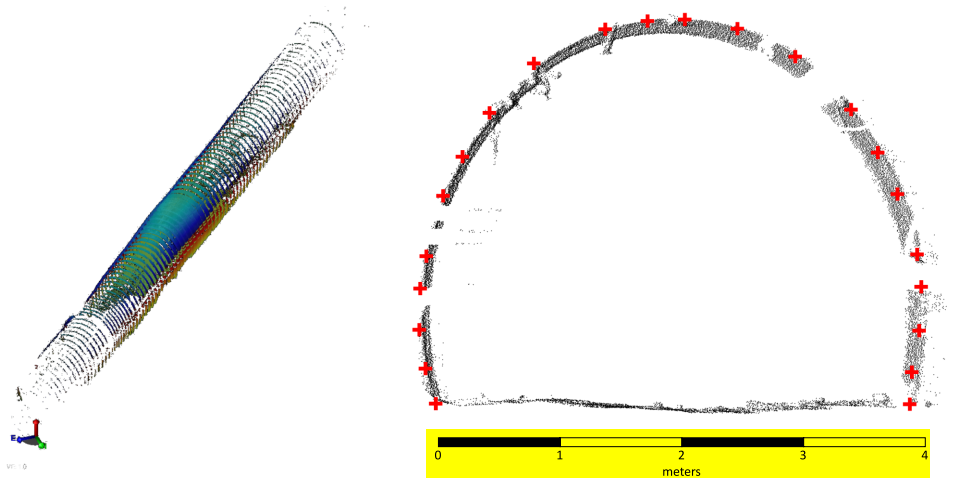

Fig. 2. 3D view of in-situ laser scanning data from the mine (case study II, left). A cross section of the mine (right) was defined by the point cloud (black) taken from the closest laser scan data. Red crosses were used as vertices of polygonal prism approximating the tunnel and modelled using the Potent software.

3. Case study I – railway tunnel Soroška

The underground gravity measurements were performed in the Jablonovský railway tunnel passing Mesozoic karst rocks in the Slovenský kras area (Fig. 3). Measurement stations in the tunnel were chosen at the crossing points of the tunnel with the former detailed surface gravity profiles (Fig. 4), while the vertical distance between surface gravity stations and the tunnel was approximately 200 m. Our goal was to validate the value of the correction density used in Bouguer anomaly calculation. Since the gravity survey mainly covers the area of Mesozoic rocks (limestones, marl slates, etc., see Fig. 4), we assumed that their density should not differ much from the value of 2.67 g/cm^3. Detailed density analysis along the surface gravity profiles based on the proportionality between free-air anomalies and the NTE (Fig. 5) confirmed this assumption, leading to the value of about 2.66 g/cm^3 (*Mikuška et al., 2017*). On the other hand, the density analysis from drilling rock-samples showed a little higher values of volume densities, specifically about 2.7 g/cm^3 (*Zahorec et al., 2017b*). We assume that this

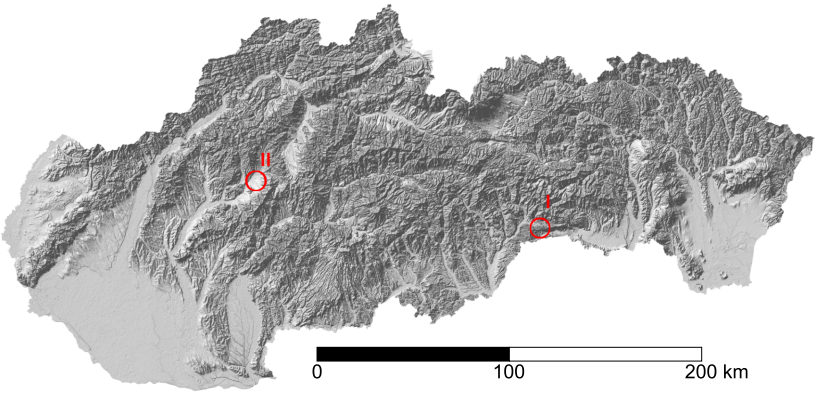

Fig. 3. Relief map of Slovakia showing position of the two studied localities with underground gravity measurements. Case study I is located in the hilly area composed of Mesozoic units of the Slovenský kras, case study II is located in the Neogene sedimentary rocks of the Hornonitrianska kotlina basin.

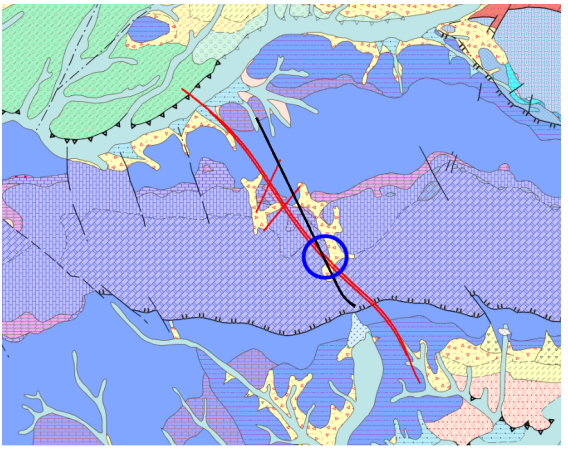

Fig. 4. Detailed situation of the case study I (blue circle). Underground gravity measurements were performed at the crossing points of railway tunnel (black line) with two parallel surface gravity profiles (longer red lines). The vicinity of the utilized measured stations is built by Steinalm and Wetterstein limestones. Geological background is taken from *Káčer et al. (2005)*.

difference could be due to a significant karstification of the limestones.

Positions of the underground gravity stations were determined by terrestrial measurements using the total station Leica MS50. Horizontal and

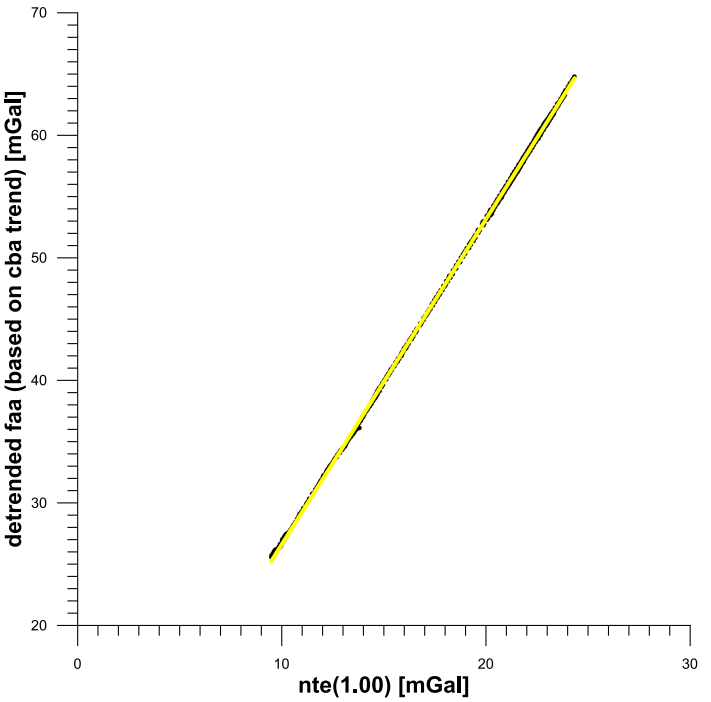

Fig. 5. Graph showing an almost linear dependence of the free-air anomalies "faa" (after elimination of a linear regional trend taken from the complete Bouguer anomaly "cba") on the near topographic effect "nte" calculated for density of 1.0 g/cm^3 (*Mikuška et al., 2017*). The linear regression coefficient of approximately 2.66 should represent the estimated density of the topographic rocks in g/cm^3 units.

vertical accuracy of the measurements are better than 0.03 m. The stations inside the tunnel were set to be vertically aligned with the surface gravity points within a few centimeters in their horizontal positions. Besides the four main stations (exactly projected from the surface gravity profiles points), several side points were also measured for comparison. Gravity values at each station were measured using CG-5 gravity meter, while the same instrument and the same methodology were used for the surface gravity measurements. The gravity measurement error was estimated at ± 10 μGal for both surface and underground measurements.

In addition, vertical gradients of gravity (VGG) were measured at two underground stations to appraise methodically the possibility of the den-

sity determination from the VGG measurements. The VGG measurements were performed in a tower mode using relative gravity meter CG-5 and a geodetic tripod. Gravity was measured in A-B-A-B-A repeated mode at two height levels (A and B) with gravity meter sensor approximately 0.25 m and 1.2 m above the ground, respectively. The exact height of the gravity meter sensor above the ground was measured using high-precision hand-held laser distance meter. The measurement at one station had to be interrupted due to a passing train. The measurement error at this station was estimated to $\pm 7\,\mu$Gal, while it was $\pm 2\,\mu$Gal at the other station.

As mentioned above, the measured positions of gravity stations and their gravity values have to be corrected for the normal gradient (–0.3086 mGal/m), and then for the NTE, including the effect of the tunnel. For this purpose we used the airborne LiDAR-based DEM with resolution of 0.5 m and estimated vertical accuracy of approximately ±0.15 m (*Zahorec et al., 2017b*). In addition, the available terrestrial laser scan model of the tunnel (performed by Amberg GRP 5000) was used for exact calculation of the effect of the tunnel. We also calculated the effect of the tunnel on the surface gravity points. Since this effect reaches values of only several μGal, it can be neglected. Tables 1 and 2 summarize the mentioned effects and the calculated density values for pairs of the surface/underground gravity stations, as well as underground VGG points. The results will be discussed

Table 1. Summarized measured differences ΔH, Δg, calculated free-air gradient effect (FAGE), near topographic effect (density of $+1.0\,\mathrm{g/cm^3}$), gravitational effect of the tunnel (density of $-1.0\,\mathrm{g/cm^3}$) and calculated densities for a set of pairs of surface/underground gravity stations within the case study I.

Under-ground station	ΔH (m)	Δg (mGal)	FAGE (mGal)	NTE surface (mGal)	NTE tunnel (mGal)	Tunnel effect (mGal)	Density ($\mathrm{g/cm^3}$)
13691	207.075	–22.367	–63.903	22.714	7.004	0.101	**2.661**
136911	207.007	–22.434	–63.882	22.714	7.013	0.118	**2.660**
13701	204.717	–22.010	–63.176	22.624	7.027	0.118	**2.659**
23801	175.836	–16.914	–54.263	21.476	7.315	0.109	**2.658**
238011	175.818	–16.933	–54.257	21.476	7.319	0.118	**2.659**
23805	175.85	–16.984	–54.267	21.476	7.332	0.118	**2.658**
23811	173.096	–16.480	–53.417	21.361	7.342	0.110	**2.656**
238111	173.103	–16.490	–53.420	21.361	7.341	0.118	**2.656**
23805	173.076	–16.453	–53.411	21.361	7.332	0.118	**2.657**

Table 2. Summarized measured differences ΔH, Δg, calculated free-air gradient effect (FAGE), near topographic effect (density of +1.0 g/cm^3), gravitational effect of the tunnel (density of –1.0 g/cm^3) and calculated densities for two gravity stations with measured vertical gradients. A stands for lower measurement level, B stands for upper level. Note that the resulting values may be subject to rounding errors.

VGG station	ΔH (m)	Δg (mGal)	FAGE (mGal)	NTE A (mGal)	NTE B (mGal)	Tunnel effect A (mGal)	Tunnel effect B (mGal)	Density (g/cm^3)
23805	0.949	–0.205	–0.293	7.353	7.431	0.118	0.071	**2.817**
136911	0.947	–0.211	–0.292	7.034	7.110	0.118	0.072	**2.723**

later.

For verification we have also compared our straightforward approach of density determination with the classical method described above (Eq. 2). Table 3 summarizes calculated effects and resultant densities. The terrain correction (for the "assumed" density of 2.67 g/cm^3) was calculated as difference between the gravitational effect of truncated spherical layer with the thickness equal to the elevation of a particular surface gravity station and the calculated NTE. We note that the this way calculated terrain correction has a "standard" meaning for surface gravity points, but this is not the case for underground gravity points. It is interesting to see that in the case of

Table 3. Summarized terrain corrections (assumed density of 2.67 g/cm^3), gravitational effects of the tunnel (assumed density of –2.67 g/cm^3) and calculated densities for a classic method applied to a set of pairs of surface/underground gravity stations (measured values of ΔH and Δg are shown in Table 1). Densities calculated for the case when terrain correction and tunnel effect are not included are shown in the last column.

Underground station	Terrain correction surface (mGal)	Terrain correction tunnel (mGal)	Tunnel effect (mGal)	Density (g/cm^3)	Density (no terrain correction) (g/cm^3)
13691	2.706	−1.629	0.269	**2.659**	**2.393**
136911	2.706	−1.638	0.315	**2.658**	**2.389**
13701	2.680	−1.430	0.316	**2.658**	**2.399**
23801	2.402	0.907	0.290	**2.656**	**2.534**
238011	2.402	0.902	0.315	**2.657**	**2.533**
23805	2.402	0.861	0.315	**2.656**	**2.529**
23811	2.396	1.133	0.294	**2.654**	**2.546**
238111	2.396	1.136	0.314	**2.654**	**2.545**
23805	2.396	1.167	0.315	**2.655**	**2.548**

underground stations, the terrain correction can reach negative as well as positive values (see third column in Table 3). That is in agreement with previous works, e.g. by *Algermissen (1961)*.

Because our goal was numerical comparison of the methods, we calculated terrain correction up to the same distance of 166.7 km, however, *Algermissen (1961)* for instance calculated his correction for topography up to 2615 m (8578 feet). The last column in Table 3 shows density values calculated for the specific case in which terrain correction and tunnel effect are not included in the calculation at all. Since this locality is hilly, the differences are significant this time.

4. Case study II – active coal mine Baňa Nováky

This case study is a typical example of an active subsidence associated with mining activities. Currently the area is intensively studied within the framework of the scientific project VEGA 1/0462/16. Monitored gravity profiles are located above the border of the mining area (Fig. 6). Unlike in case study I, a small number of the monitored gravity points, as well as the flatness of the area, do not allow a reliable density analysis based on the surface gravity profiles. Moreover, we do not have rock-sample density analysis available from this area. Therefore we performed underground gravity measurements (and corresponding surface measurements) in accessible mining corridors, in order to prove the density determination methodology and to better estimate the Bouguer correction density for the gravity profiles.

Positions of five underground gravity stations (Fig. 6) were determined by terrestrial measurements using the total station Trimble SX10. Horizontal and vertical accuracies of the measurements are better than 0.05 m. The corresponding surface gravity stations were targeted using GNSS measurement in the Real Time Kinematic Mode (RTK) with SKPOS service. The surface stations were set to be vertically aligned with the underground gravity stations within a few centimeters in horizontal position, while the vertical distance between surface/underground stations ranged from 146 to 200 m.

Gravity value at each station was measured using two CG-5 gravity meters. After the data processing we found out that there were systematic

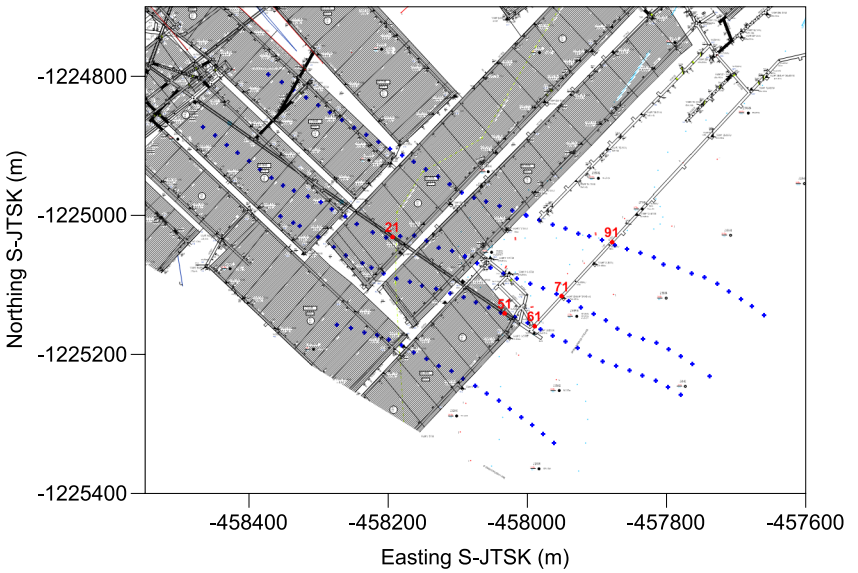

Fig. 6. Situation of the case study II. Red numbered circles represent pairs of surface/underground gravity stations. Blue crosses are surface monitoring gravity profiles. Shaded background indicates excavated coal beds. Underground measurements were carried out in mining corridors, which are also visible.

differences between the gravity values from the individual gravity meters (average difference of 40 μGal). We assumed that this could be caused by incorrect calibration factors of gravity meters. Therefore we subsequently performed re-calibration of both gravity meters at vertical calibration line with gravity range of 200 mGal in the High Tatra Mountains. After the reprocessing, average difference between gravity values from both gravity meters decreased from 40 to 15 μGal. It is even more interesting to note that *McCulloh (1965)* already pointed out the errors in density determination associated with bad calibration factors.

Besides positional measurements, we also used total station Trimble SX10 for laser scanning to map the shape and dimensions of the mining corridors in order to calculate their effect using the Toposk program. However, it was not easily performed because of the presence of dense fog. We got sufficient scans (at least 20 m around the gravity station) only at two stations. Therefore we had to model the gravitational effect of the corri-

dors also in another way, by means of polygonal prism approximation using the software Potent (Fig. 7), while a cross-section of the prism was defined on the basis of laser scan data (Fig. 2). We compared both approaches at common points. Both methods provided practically the same results. The advantage of the modelling via Potent software is that we can extend the length of the corridor arbitrarily. On the other hand, proved by our modelling tests, extending the corridor length beyond 20 m on both sides brings only negligible improvement of its gravitational effect.

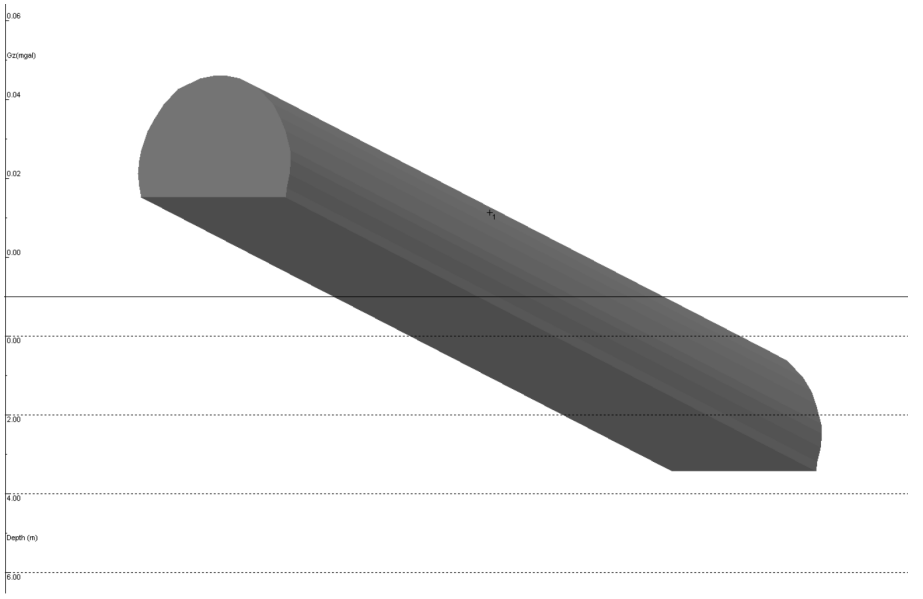

Fig. 7. Mining corridor modelled in Potent software (picture is taken from software interface).

The NTE was calculated in the same way as described above, using high-precision airborne LiDAR-based DEM, although this time with resolution of 1 m and estimated vertical accuracy of approximately ±0.15 m. The calculated effects are summarized in Table 4. The average value of the determined density is about 2.04 g/cm^3. According to *Šamajová and Hók (2018)*, densities in Neogene basins should range from 2.0 to 2.2 g/cm^3 to a depth of 1000 m. Nevertheless, *Stránska et al. (1986)* state the value of 1.92 g/cm^3 for Neogene formation in Hornonitrianska kotlina basin.

Table 4. Summarized measured differences ΔH, Δg, calculated free-air gradient effect (FAGE), near topographic effects (density of $+1.0\,\mathrm{g/cm^3}$), gravitational effects of the mining corridor (density of $-1.0\,\mathrm{g/cm^3}$) and calculated densities for a set of pairs of surface/underground gravity stations in case study II.

Station	ΔH (m)	Δg (mGal)	FAGE (mGal)	NTE surface (mGal)	NTE mine (mGal)	Mine effect (mGal)	Density ($\mathrm{g/cm^3}$)
21	200.252	−27.242	−61.798	11.447	−5.765	0.052	**2.014**
51	147.994	−20.077	−45.671	11.718	−0.956	0.053	**2.028**
61	146.02	−19.747	−45.062	11.831	−0.639	0.064	**2.041**
71	147.958	−19.913	−45.660	11.885	−0.719	0.066	**2.054**
91	150.308	−20.015	−46.385	11.914	−0.884	0.060	**2.070**

5. Discussion

Results from case study I (Table 1) show that the surface/underground gravity measurements give reliable density value of approximately $2.66\,\mathrm{g/cm^3}$, which is in perfect agreement with the density analysis of profile surface measurements (Fig. 5). This density value also supports the assumption about the lower mean density due to the karstification of the rocks, in contrast to the laboratory rock-samples densities. There is yet another interesting fact arising from Table 1. We can sort the measured stations into two groups according to their position below the surface profiles. The first group consists of the first three points (numbered starting with the numeral 1). This group of points is about 300 m away from the second group along the tunnel. When considering these groups separately, we can see a weakly decreasing trend of the calculated density. The average density value in the first group of points is $2.660\,\mathrm{g/cm^3}$, while in the second group it is $2.657\,\mathrm{g/cm^3}$. The difference is really small, but it could represent a change in lithology, or in the intensity of karstification.

On the contrary, underground VGG measurements (Table 2) show controversial results. The estimated densities differ from each other, as well as from previous values. This could have several reasons. First reason could be the expected sensitivity of the method to the measurement error. Table 2 shows that the greatest impact on the mutual density differences between two stations arises from the measured gravity differences. Better density estimation would require more accurate VGG measurements. Yet

there is also another issue to consider. The VGG measurement, unlike the surface/underground measurement, is much more sensitive to local density conditions around the VGG station. This makes the method principally less suitable for Bouguer correction density estimation, even if the maximum measurement accuracy is achieved.

Comparing densities calculated using the presented method (Table 1) with the ones calculated using the classical method (Table 3, fifth column), we found only very small differences. This is because we used the same approach for the calculation of the NTE and the terrain correction and also because the "assumed" density of 2.67 g/cm^3 (used for terrain correction in the classical method) is very close to the true density. However, if the assumed density differed greatly from the real one, the result would be much more affected. This fact is highlighted when the terrain corrections in the classical method are completely omitted (Table 3, last column). Since the topography in this area is hilly, the error in density estimation increases considerably.

Densities determined in the case study II (Table 4) show a significantly increasing trend with increasing number of stations. We assume that there could actually be a connection with the positions of stations, since the stations with lower numbers are distributed in the area of extracted coal beds, while those with higher numbers are outside the exploited area (see Fig. 6).

One more remark is needed. The presented method is easy to implement in cases where underground stations are still at positive heights (i.e. above sea level), which was the case for both presented sites. On the other hand, if underground stations would have negative heights (i.e. below sea level), the method would require modifying elevation models, because usually DEMs are defined only for positive elevations.

6. Conclusions

The presented straightforward method for Bouguer correction density determination based on underground as well as surface gravity measurements was used in two case studies with different conditions. The density of 2.66 g/cm^3 was calculated for a Mesozoic karst area in the Slovenský kras and the mean density of 2.04 g/cm^3 was calculated for the Neogene rocks of the Hornonitrianska kotlina basin. The determined densities are in accordance with

the published values typical for both sites. At the first site a slightly lower density was determined compared to the results of rock-samples analysis, probably due to karstification. In addition, the calculated densities show systematic change in horizontal direction, suggesting the possible change in the geological structure depending on the position of extracted coal beds (case study II), as well as the intensity of karstification (case study I). Comparison with the "classical" method (based on Poincaré-Prey reduction including terrain corrections) shows consistency, if the same approach is used for the topographic effect and the terrain correction calculation. On the contrary, if the terrain corrections are omitted or calculated with incorrectly assumed density, the possible error from the classical approach will arise. Therefore the presented method is not only simpler but also more reliable than the classical method.

Acknowledgements. This work was supported by the VEGA grant agency under project No. 1/0462/16. The authors express their thanks to Marián Plakinger (Hornonitrianske bane Prievidza), Matej Oros (Geotronics Slovakia), Branislav Hinca, Vladimír Minarech (REMING CONSULT) and Martin Salva (Železnice Slovenskej republiky) for assistance with the realization of the measurements.

References

Algermissen S. T., 1961: Underground and surface gravity survey, Leadwood, Missouri. Geophysics, **26**, 158–168.

Domzalski W., 1955: Relative determination of the density of surface rocks and the mean density of the Earth from vertical gravity measurements. Geophysical prospecting, **3**, 212–227.

Hammer S., 1950: Density determination by underground gravity measurements. Geophysics, **15**, 637–652.

Hinze W. J., Aiken C., Brozena J., Coakley B., Dater D., Flanagan G., Forsberg R., Hildebrand T., Keller G. R., Kellogg J., Kucks R., Li X., Mainville A., Morin R., Pilkington M., Plouff D., Ravat D., Roman D., Urrutia-Fucugauchi J., Véronneau M., Webring M, Winester D., 2005, New standards for reducing gravity data: The North American gravity database. Geophysics, **70**, J25–J32.

Káčer Š., Antalík M., Lexa J., Zvara I., Fritzmann R., Vlachovič J., Bystrická G., Brodianska M., Potfaj M., Madarás J., Nagy A., Maglaj J., Ivanička J., Gross P., Rakús M., Vozárová A., Buček S., Boorová D., Šimon L., Mello J., Polák M., Bezák V., Hók J., Teťák F., Konečný V., Kučera M., Žec B., Elečko M., Hraško Ľ., Kováčik M., Pristaš J., 2005: Digital geological map of Slovak Republic in the scale 1:50 000. Final report, State Geological Institute of Dionýz Štúr, Bratislava.

LaFehr T. R., 1991: Standardization in gravity reduction. Geophysics, **56**, 1170–1178.

McCulloh T. H., 1965: A confirmation by gravity measurements of an underground density profile based on core densities. Geophysics, **30**, 1108–1132.

Mikuška J., Marušiak I., Zahorec P., Papčo J., Pašteka R., Bielik M., 2014: Some Interesting Facts about Correlation between Gravity Anomalies and Heights with Implications towards the Bouguer Correction Density Estimation. AGU FALL MEETING, San Francisco, 15–19 December 2014 (poster).

Mikuška J., Zahorec P., Papčo J., Karcol R., Marušiak I., 2017: Surface rock density interpretation from detailed gravity measurements based on free-air anomalies and near topographic effects in a terrain with sufficient relative relief. XII Slovak Geophysical Conference, 28–29 September, 2017, Bratislava (oral, abstract).

Nettleton L. L., 1939: Determination of density for reduction of gravimeter observations. Geophysics, **4**, 176–183.

Pícha J., 1953: Underground gravity acceleration in the mine "Anna" in Březové hory Mountain. Travaux géophysiques, **9**, Geophysical Institute ČSAV, Praha, 119–129.

Pospíšil L., Černota P., Mikuška J., Volařík T., Pospíšil J., Papčo J., Zahorec P., 2013: Experimental gravity and vertical gravity gradient measurements in mine shaft Stonava (Sto-Su-1), Ostrava-Karviná district, Czech Republic. Workshop "Tatry 2013 – New pieces of knowledge based on realizing and interpreting geodetic observations", 21–22 November, 2013, Štrbské pleso, High Tatras, Slovakia (oral). ISBN 978-80-89626-01-4.

Potent v.4.11.06, 2010: User guide. Manuscript, Geophysical Software Solutions Pty. Ltd., Gungahlin, Australia.

Schiavone D., Capolongo D., Loddo M., 2009: Near-station topographic masses correction for high-accuracy gravimetric prospecting. Geophysical Prospecting **57**, 739–752.

Stránska M., Ondra P., Husák Ľ., Hanák J., 1986: Density map of the West Carpathians within the territory of Czechoslovakia. Final report, Geofyzika s.e. Brno, branch Bratislava, (unpublished; in Slovak).

Šamajová L., Hók J., 2018: Densities of rock formations of the Western Carpathians on the territory of Slovakia. Geological Studies, Reports, **132**, State Geological Institute of Dionýz Štúr, Bratislava. (in press; in Slovak).

Vybíral V., Jančí J., Maar S., 1990: Nízke Tatry Mountains – Jasenie Au, W. Geophysical survey – III phase (1989–1990). Final report, Geofyzika s.e. Brno, branch Bratislava (unpublished; in Slovak).

Zahorec P., Vajda P., Papčo J., Sainz-Maza S., Pereda de Pablo J., 2016: Prediction of vertical gradient of gravity and its significanse for volcano monitoring – example from Teide volcano. Contributions to Geophysics and Geodesy, **46**, 3, 203–220.

Zahorec P., Marušiak I., Mikuška J., Pašteka R., Papčo J., 2017a: Numerical Calculation of Terrain Correction Within the Boguer Anomaly Evaluation (Program Toposk), chapter 5, pp. 79–92, In book: Roman Pašteka, Ján Mikuška and Bruno Meurers (Eds.): Understanding the Bouguer Anomaly: A Gravimetry Puzzle, Elsevier, ISBN 978-0-12-812913-5, doi: 10.1016/B978-0-12-812913-5.00006-3.

Zahorec P., Papčo J., Vajda P., Szabó S., 2017b: Realization of geophysical survey – gravimetry within the project "Highway R2 Rožňava – Jablonov nad Turňou". Technical report, Slovak Academy of Sciences, Earth Science Institute, Banská Bystrica (unpublished; in Slovak).

sciendo

Contributions to Geophysics and Geodesy Vol. 48/4, 2018 (337–348)

The National Network of Seismic Stations of Slovakia – Current state after 13 years in operation from the project of modernization and enhancement

Kristián CSICSAY[1,*], Andrej CIPCIAR[1,2], Lucia FOJTÍKOVÁ[1,3], Miriam KRISTEKOVÁ[1,2], Martin GÁLIS[1,2], Miroslav SRBECKÝ[1], Zuzana CHOVANOVÁ[1], Erik BYSTRICKÝ[1], Róbert KYSEL[1,2]

[1] Earth Science Institute of the Slovak Academy of Sciences, Dúbravská cesta 9, P. O. Box 106, 840 05 Bratislava, Slovak Republic

[2] Faculty of Mathematics, Physics and Informatics Comenius University in Bratislava, Mlynská dolina, 842 48 Bratislava, Slovak Republic

[3] Institute of Rock Structure and Mechanics of the Czech Academy of Sciences, V Holesovickach 94/41, 182 09, Prague 8, Czech Republic

Abstract: We present the state of the modernized, upgraded and enhanced National Network of Seismic Stations (NNSS) of Slovakia at the end of the year 2017 and the importance of the Project: Modernization and enhancement of the National Network of Seismic Stations which took place in years 2001–2004. In this period some stations were modernized and upgraded and several new stations were built in various places in Slovakia to increase ability to localize seismic events on the territory of Slovakia and adjacent areas. Before the year 2001 the average number of localized earthquakes on the territory of Slovakia was only 7 per year. The breakthrough occurred in the year 2005 with the fully operational network when the number of localized earthquakes with epicentre on the territory of Slovakia was increased up to 50. Now this number is approximately 70–90 earthquakes per year. We present the changes in the NNSS in the last 13 years, obtained results (some of them are preliminary), advantages and weaknesses of the NNSS and future plans toward further improvements of our seismic network system.

Key words: Slovakia, National Network of Seismic Stations, earthquakes

1. Introduction

Before the year 2001 the NNSS consisted of six permanent seismic stations – Hurbanovo (HRB), Košice (KOS), Modra (MOD), Šrobárová (SRO), Vyhne

*corresponding author: e-mail: kristian.csicsay@savba.sk

doi: 10.2478/congeo-2018-0016

(VYH) and Železná studnička (ZST) (Fig. 1). Due to the quality of seismic records and number and placement of seismic stations the ability to localize seismic events was at very low level (*Moczo et al., 2005*). The average number of localized earthquakes on the territory of Slovakia was only 7 per year (*Cipciar et al., 2017*). In the year 2001 a new very important and ambitious project was started which primary goal was to upgrade the NNSS to the standard European level at that time. The NNSS has been modernized and enhanced during the years 2001–2004. The Železná studnička seismic station was the only one at the European level at that time and only minimal upgrade was necessary. All other seismic stations (Modra, Šrobárová, Vyhne) required serious upgrades. Due to increased noise level, the seismic station Košice was cancelled from operation and moved to Červenica, where was a more suitable place for seismic recording. New seismic stations Iža, Kečovo, Kolonické sedlo, Likavka, Moča, Stebnícka Huta were built (*Moczo et al., 2005*). For each new seismic station a site selection process was car-

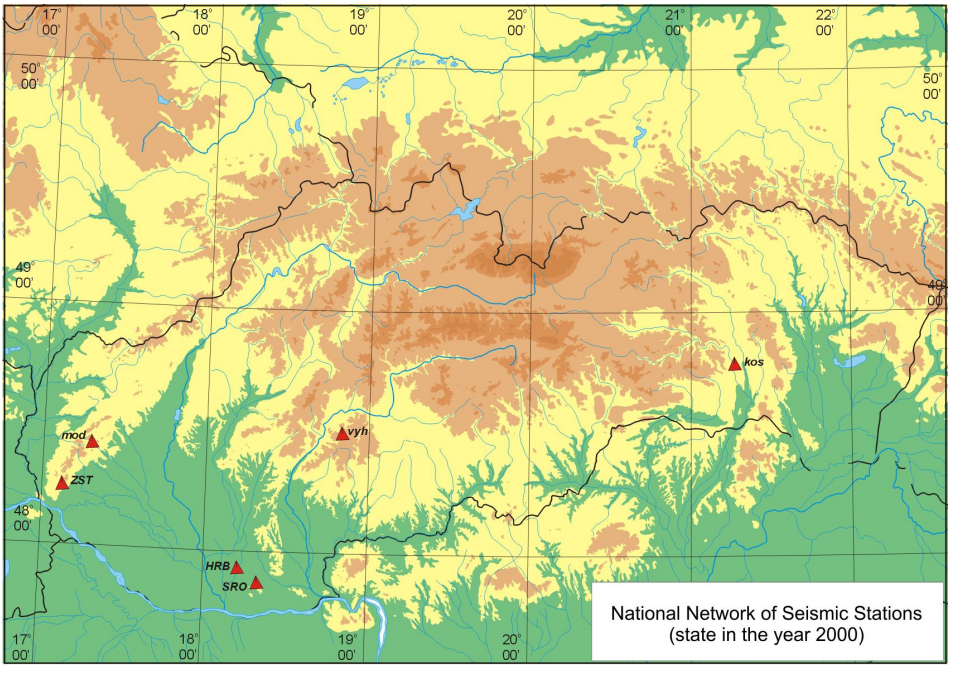

Fig. 1. State of the NNSS in the year 2001 after *Moczo et al. (2005)*.

ried out. A typical seismic station was equipped with a sensor (short period or broadband), 16bit digitizer, GPS, classic PC and satellite. Only the oldest seismic station Hurbanovo was not upgraded during the project. This seismic station has been in operation since 1909 (*Pajdušák, 1997*) and is equipped with two horizontal seismographs type Mainka and analogue registration on a smoked paper. After the end of the Project: Modernization and enhancement of the National Network of Seismic Stations the NNSS consisted of five broadband and seven short period seismic stations (Fig. 2) (*Moczo et al., 2005*). For more information about the beginnings and initial status of the modernized and enhanced NNSS see paper *Labák (2004)*.

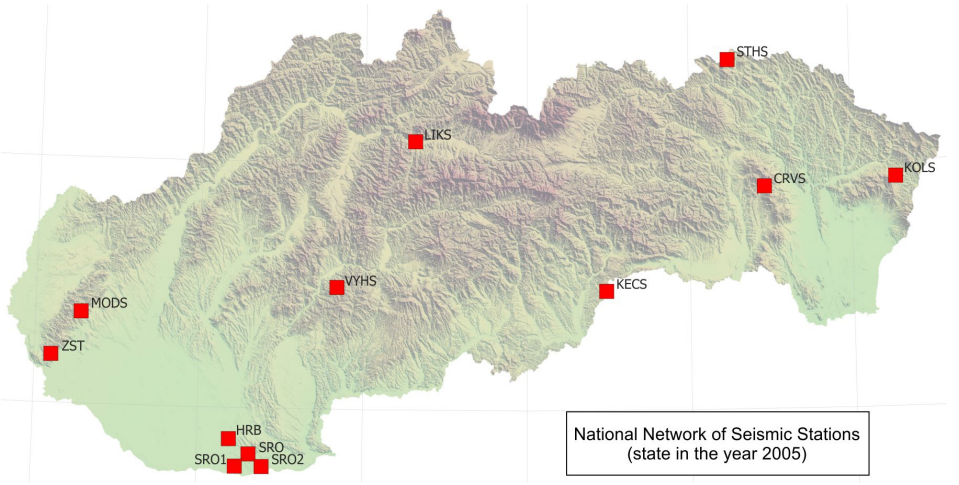

Fig. 2. State of the NNSS after the end of the Project: Modernization and enhancement of the National Network of Seismic Stations.

2. Current state of the NNSS

At the present, the NNSS (*ESI SAS, 2004*) is the most important Slovak infrastructure for monitoring of seismic activity. Its main mission and goal is to monitor and localize earthquakes with macroseismic effects (effects on people, objects, buildings and nature) on the territory of Slovakia. Besides these earthquakes the seismic stations of NNSS record also weaker local

earthquakes and other seismic events (e.g. quarry blasts) as well as regional end teleseismic earthquakes and nuclear explosions. All permanent seismic stations are registered in the International Seismological Centre (ISC).

The network consists of eight short period and five broadband seismic stations (Fig. 3). Broadband stations are: Červenica (CRVS), Kolonické sedlo (KOLS), Modra (MODS), Vyhne (VYHS) and Železná studnička (ZST). Short period seismic stations are: Hurbanovo (HRB), Izabela (IZAB), Iža (SRO1), Kečovo (KECS), Liptovská Anna (LANS), Moča (SRO2), Stebnícka Huta (STHS) and Šrobárová (SRO). Some of them are in operation with original equipment since the installation, others have undergone upgrading process partly or completely (e.g. 24/32bit digitizers, 12V mini-PC). Due to signal problem caused by increased level of background seismic noise the seismic station Likavka (LIKS) have been moved to the new location in Liptovská Anna in cooperation with the Progseis, Ltd. company in the year 2009 (Fig. 4). Almost 9 years of operation the Liptovská Anna (LANS) proves to be our best short period seismic station. In the year 2016 the seismic station IZAB has been added to the NNSS as a new permanent short period seismic station. This seismic station has been operated in cooperation with Progseis, Ltd. company. Three additional stations Banka (BAN), Podolie (POD), Jalšové (JAL) have been added to the NNSS in

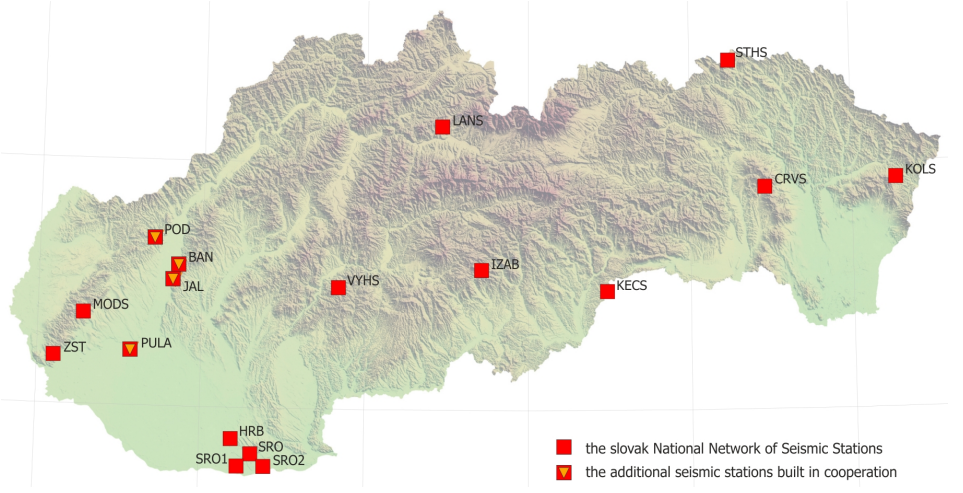

Fig. 3. Current state of the NNSS.

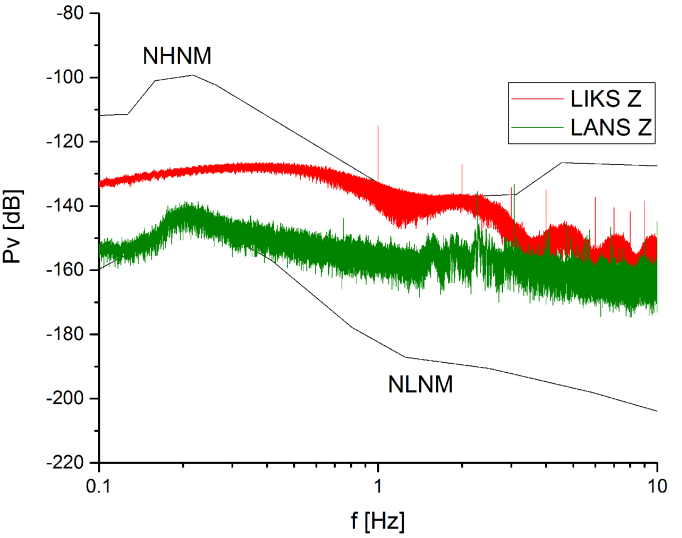

Fig. 4. Comparison of the data quality on the component Z of the seismic stations LIKS and LANS. NHNM and NLNM model is after *Bormann and Wielandt (2002)*. NHNM – new high noise model, NLNM – new low noise model, Pv – velocity power spectral density.

the Little Carpathians (Fig. 3) in cooperation with Progseis, Ltd. company and Institute of Rock Structure and Mechanics of the Czech Academy of Sciences (*Fojtíková et al., 2015*). The seismic station Pusté Úľany (PULA) has been added to the NNSS in Podunajská nížina (Fig. 3) in cooperation with Institute of Rock Structure and Mechanics of the Czech Academy of Science.

Three basic types of stations can be classified: cave, vault and surface stations. The cave type stations are CRVS, IZAB, MODS, VYHS, ZST and these stations are mostly broadband stations. The vault type stations are KOLS, SRO, SRO1, SRO2, STHS.These seismic stations are short-period except KOLS, where a broadband sensor is installed. The surface stations, which are equipped with short-period sensors, are BAN, HRB, JAL, KECS, LANS, POD and PULA. For more details about seismic stations and their equipment see the website `http://www.seismology.sk`.

The data are transmitted from all seismic stations in real-time, except HRB – the reason mentioned above and are collected by the software pack-

age SeisComp3 (*Weber et al., 2007*) through SeedLink server. For routine daily interpretation of collected data the Seismic Handler software package (*Stammler, 1993*) is used. Continuous raw seismic data from the NNSS are stored in a local archive and seismic data interpretations (together with information on equipment of stations) are stored in a web accessible database. Beside seismic data from the NNSS we also use seismic data from other local networks in Slovakia (*Local Seismic Network of Eastern Slovakia*, two private local seismic networks around nuclear power plants Jaslovské Bohunice and Mochovce) and seismic data from networks of neighbouring countries - Austrian Seismic Network (*ZAMG – Zentralanstalt für Meterologie und Geodynamik, 1987*), Czech Regional Seismic Network (*Institute of Geophysics, Academy of Sciences of the Czech Republic, 1973*), Hungarian National Seismological Network (*Kövesligethy Radó Seismological Observatory, 1992*), Local seismological network for monitoring NPP Dukovany (*Institute of Physics of the Earth Masaryk University, 2014*), GEOFON Seismic Network (*GEOFON Data Center, 1993*), *Polish Seismological Network*.

Daily seismic data from the NNSS are provided to the ORFEUS Data Center through GEOFON Data Center in Potsdam (*GEOFON Data Center, 1993*). From there other countries and institutions can download and use these data. Seismic data from the NNSS are used permanently for the daily interpretation of seismic events by neighbouring countries e.g. *Bondár et al. (2018); Schneider et al. (2018); Yang et al. (2018).*

All permanent seismic stations of the NNSS are included in the Central and East European Earthquake Research Network – CE^{3}RN (*Lenhardt et al., 2014*) and three broadband stations MODS, VYHS and ZST are part of the AlpArray permanent seismic network (*Hetényi et al., 2018*).

3. Preliminary results and results

Although the Project: Modernization and enhancement of the National Network of Seismic Stations had indicated positive results already in the year 2004, the real breakthrough occurred in the year 2005 with the fully operational network. In this year the number of interpreted seismic events and phases (Graph 1) and localized earthquakes on the territory of Slovakia (Graph 2) increased dramatically compared to the year 2003 and sooner.

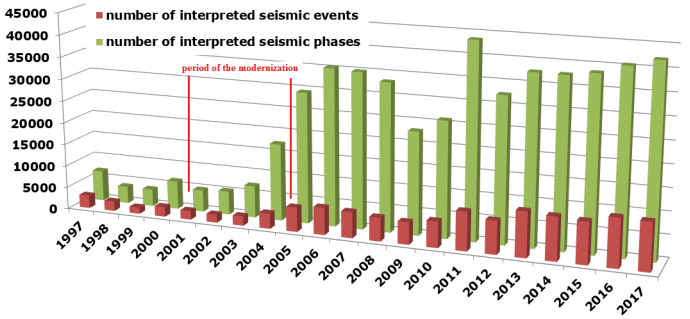

Graph 1. Number of interpreted seismic events and phases in the period 1995–2017.

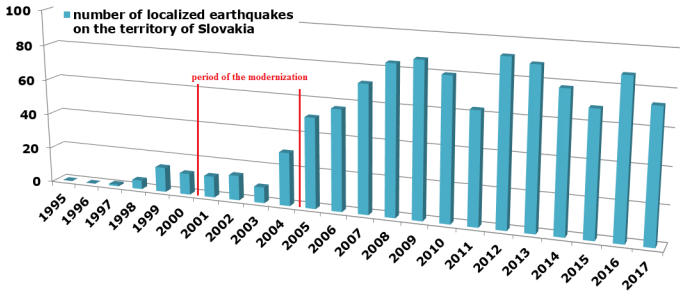

Graph 2. Number of localized earthquakes on the territory of Slovakia in the period 1995–2017.

Other very appropriate comparison of the old and the new NNSS is the ability to seismometrically localize earthquakes on the territory of Slovakia. Fig. 5 shows the number of seismometrically localized earthquakes in the period 1902–2003. During this period only 92 earthquakes were seizmometrically localized. Recently approximately 70–90 earthquakes with epicentre on the territory of Slovakia are localized every year, most of them (cca 97%) are weak events with estimated local magnitudes below 2 (*Cipciar et al., 2017*).

The increase accuracy of localizations of earthquakes on the territory of Slovakia allows more precise definition of seismo-active areas and their active fault systems and helps us to eliminate mining events from the earthquake catalogue (Fig. 6). Thanks to modernized and enhanced seismic network,

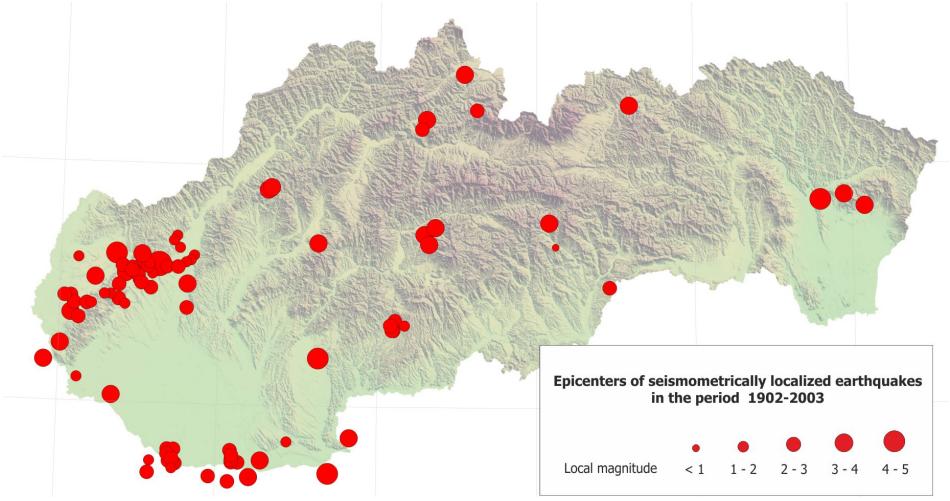

Fig. 5. Epicentres of seismometrically localized earthquakes on the territory of Slovakia by the old NNSS in the period 1902–2003.

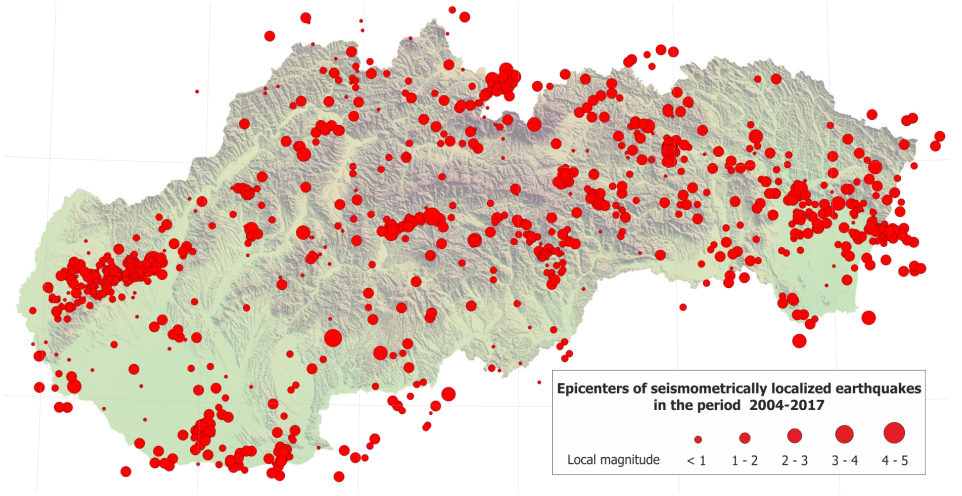

Fig. 6. Epicentres of seismometrically localized earthquakes on the territory of Slovakia and adjacent areas by the new NNSS in the period 2004–2017.

localizations of earthquake epicentres confirm geological neotectonic and recently active fault zones (e.g. *Fojtíková et al., 2010; Hók et al., 2014, 2016, 2018; Madarás et al., 2012; Marko et al., 2017*). The hypocentres of these earthquakes indicate shallow earthquake activity on the territory of Slovakia with a maximum depth to 15 km. We plan common geological and geophysical interpretation of the localized earthquakes together with geologists in the future.

The increased number of recorded and localized earthquakes by modernized NNSS allowed the determination of the new local magnitude formulae for the territory of Slovakia (*Chovanová and Kristek, 2018*). Until now the (*Hutton and Boore, 1987*) formula was used for estimation of the local magnitudes. One of the main motivations of developing the new formulae was the reduction of the differences between the local magnitudes estimated for one event at different seismic stations of the NNSS. The formulae was developed using 3579 trace amplitudes recorded by nine permanent seismic stations of the NNSS from 2005 until 2016. The formulae are valid from 10 km up to 550 km of epicentral distance. The attenuation parameters and also the station corrections for nine seismic stations were estimated. The range of the station corrections is –0.21 for VYHS up to 0.28 for KOLS. The smallest correction 0.03 is for CRVS and MODS station. Using the new formulae with the station corrections, the reduction of error is up to 58% comparing to formulae by *Hutton and Boore (1987)*.

4. Conclusion and discussion

Period of 13 years of the seismic activity monitoring on the territory of Slovakia from a geological point of view is very short time but years 2004–2017 show enormous advances to understanding the seismic regime of active fault systems and geological evolution of tectonic units on the territory of Slovakia. Currently the new NNSS localize approximately ten times more earthquakes on the territory of Slovakia then the old NNSS. Localizations of earthquake epicentres confirm geological neotectonic and recently active fault zones.

However, the seismic monitoring in Slovakia should be further improved. Due to lack of strong earthquakes and missing temporary stations in the

main seismo-active areas (except for the Little Carpathian seismic source zone), the ability of the calculation of focal mechanisms is at very low level. Recent years of data acquisition and processing showed the necessity to build additional stations in various parts of Slovakia, particularly in Spiš and Kysuce – Orava regions from where still we don't have enough information about the seismic regime in these seismo-active areas. On the other hands 13 years of monitoring is too much for seismological equipment. For this reason we need to replace outdated seismometers and data loggers with new modern instruments.

The results of seismic monitoring in Slovakia before and after modernization clearly demonstrate a success of the realization of the Project: Modernization and enhancement of the National Network of Seismic Stations and it's importance for a future seismological and tectonic research of the Slovak territory and adjacent areas.

Acknowledgements. The authors have been supported by the Slovak Foundation Grant VEGA 2/0188/15 and The Slovak Research and Development Agency Grant APVV-16-0146. The authors are thankful to prof. Peter Moczo for the realization and management of the Project: Modernization and enhancement of the National Network of Seismic Stations and also to other members of the team who contributed to modernization and helped to improve the operation of the National Network of Seismic Stations.

References

Bondár I., Mónus P., Czanik Cs., Kiszely M., Gráczer Z., Wéber Z., AlpArray Working Group, 2018: Relocation of Seismicity in the Pannonian Basin Using a Global 3D Velocity Model. Seismological Research Letters, **89**, 6, 2284–2293, doi: 10.1785/0220180143.

Bormann P., Wielandt E., 2002: Chapter 4: Seismic Signals and Noise (Version June 2013) In: Bormann P. (Ed.) 2002. IASPEI New Manual of Seismological Observatory Practice. GeoForschungsZentrum Potsdam, **1**, 7, 1–62, doi: 10.2312/GFZ.NMSOP-2_ch4.

Chovanova Z., Kristek J., 2018: A Local Magnitude Scale for Slovakia, Central Europe. Bulletin of the Seismological Society of America, **108**, 5A, 2756–2763, doi: 10.1785/0120180059.

Cipciar A., Chovanová Z., Csicsay K., Kristeková M., Fojtíková L., Kysel R., Pažák P., Srbecký M., Bystrický E., Gális M., Kristek J., Moczo P., 2017: Slovak Earthquakes Catalogue, Version 2017. Earth Science Institute of the Slovak Academy of Sciences.

ESI SAS (Earth Science Institute of the Slovak Academy of Sciences), 2004: National Network of Seismic Stations of Slovakia. Deutsches GeoForschungsZentrum GFZ, Other/Seismic Network, doi: 10.14470/FX099882.

Fojtíková L., Vavryčuk V., Cipciar A., Madarás J., 2010: Focal mechanisms of microearthquakes in the Dobrá Voda seismo-active area in the Malé Karpaty Mts. (Little Carpathians), Slovakia. Tectonophysics, **492**, 213–229.

Fojtíková L., Kristeková M., Málek J., Sokos E., Csicsay K., Záhradník J., 2015: Quantifying capability of a local seismic network in terms of locations and focal mechanism solutions of weak earthquakes. Journal of Seismology, **20**, 1, doi: 10.1007/s10950-015-9512-1.

GEOFON Data Center, 1993: GEOFON Seismic Network. Deutsches GeoForschungsZentrum GFZ, Other/Seismic Network, doi: 10.14470/TR560404.

Hetényi Gy., Molinari I., Clinton J., Bokelmann G., Bondár I., Crawford W. C, Dessa J.-X., Doubre C., Friederich W., Fuchs F., Giardini D., Gráczer Z., Handy M. R., Herak M., Jia Y., Kissling E., Kopp H., Korn M., Margheriti L., Meier T., Mucciarelli M., Paul A., Pesaresi D., Piromallo C., Plenefisch T., Plomerová J., Ritter J., Rümpker G., Šipka V., Spallarossa D., Thomas Ch., Tilmann F., Wassermann J., Weber M., Wéber Z., Wesztergom V., Živčić M., AlpArray Seismic Network Team, AlpArray OBS Cruise Crew, AlpArray Working Group, 2018: The AlpArray seismic network: A large-scale European experiment to image the Alpine orogen. Surveys in Geophysics, **39**, 5, 1009–1033, doi: 10.1007/s10712-018-9472-4.

Hók J., Šujan M., Šipka F., 2014: Tectonic division of the Western Carpathians: an overview and a new approach. Acta Geologica Slovaca, **6**, 2, 135–143. (in Slovak with English Summary).

Hók J., Kysel R., Kováč M., Moczo P., Kristek J., Kristeková M., Šujan M., 2016: A seismic source zone model for the seismic hazard assessment of Slovakia. Geologica Carpathica, **67**, 3, 273–288.

Hók J., Littva J., Šujan M., Šamajová L., Šujan M., Šipka F., 2018: Geological structure of the Dobrá Voda seismoactive area (western Slovakia). Acta Geologica Slovaca, **10**, 2, in press.

Hutton L., Boore D. M., 1987: The ML scale in southern California, Bulletin of the Seismological Society of America, **77**, 2074–2094.

Institute of Geophysics, Academy of Sciences of the Czech Republic, 1973: Czech Regional Seismic Network. International Federation of Digital Seismograph Networks, Other/Seismic Network, doi: 10.7914/SN/CZ.

Institute of Physics of the Earth Masaryk University (Czech), 2014: IPE_EDU. International Federation of Digital Seismograph Networks, Other/Seismic Network, doi: 10.7914/SN/D1.

Kövesligethy Radó Seismological Observatory (Geodetic and Geophysical Institute, Research Centre for Astronomy and Earth Sciences, Hungarian Academy of Sciences (MTA CSFK GGI KRSZO)), 1992: Hungarian National Seismological Network. Deutsches GeoForschungsZentrum GFZ. Other/Seismic Network, doi: 10.14470/UH028726.

Labák P., 2004: Slovak National Network of Seismic Stations - an overview. Geophysical Instute, Slovak Academy of Sciences, 8, http://www.fdsn.org/media/meetings/2004/Slovak_FDSN_2004.pdf.

Lenhardt W., Pesaresi D., Živčić M., Costa G., Kuk K., Bondár I., Duni L., Spacek P., Dimitrova L., Popa M., 2014: Central and East European Earthquake Research Network. International Federation of Digital Seismograph Networks, Other/Seismic Network, doi: 10.7914/SN/C3.

Local Seismic Network of Eastern Slovakia. Faculty of Mathematics, Physics of the Earth and Informatics, Comenius University, http://www.fyzikazeme.sk/mainpage/index_en.htm.

Madarás J., Fojtíková L., Hrašna M., Petro Ľ., Ferianc, D., Briestenský M., 2012: Definition of the seismic active regions in Slovakia based on historical earthquake records and current monitoring of tectonic and seismic activity. Mineralia Slovaca, **44**, 351–364. (in Slovak, English resume).

Marko F., Andriessen P. A. M., Tomek Č., Fojtíková L., Bošanský M., Piovarči M., Reichwalder P., 2017: Carpathian Shear Corridor – A strike-slip boundary of an extruded crustal segment. Tectonophysics, **703–704**, 119–134, doi: 10.1016/j.tecto.2017.02.010.

Moczo P., Labák P., Kristek J., 2005: Modernizácia a doplnenie Národnej siete seizmických staníc. Záverečná správa za celú dobu riešenia projektu 2/9011/21. Geofyzikálny ústav Slovenskej akadémie vied, Bratislava, 36 (in Slovak).

Pajdušák P., 1997: Historical seismic instrumens at the stations Hurbanovo (HRB) and Skalnaté pleso (SPC) of Slovakia. Cahiers du Centre Européen de Géodynamique et de Séismologie, **13**, 49–60.

Polish Seismological Network (PLSN), Institute of Geophysics Polish Academy of Sciences, https://www.igf.edu.pl/stacje-en.php.

Schneider F. M., Fuchs F., Kolinsky P., Caffagni E., Dorninger M., Serafin S., Bokelmann G., AlpArray Working Group, 2018: Seismo-acoustic signals of the Baumgarten (Austria) gas explosion detected by the AlpArray seismic network. Earth and Planetary Science Letters, **502**, 104–114, doi: 10.1016/j.epsl.2018.08.034.

Stammler K., 1993: Seismichandler-Programmable multichannel data handler for interactive and automatic processing of seismological analyses. Computers & Geosciences, **19**, 2, 135–140, doi: 10.1016/0098-3004(93)90110-Q.

Yang L., Stehly L., Paul A., AlpArray Working Group, 2018: High-resolution surface wave tomography of the European crust and uppermost mantle from ambient seismic noise. Geophysical Journal International, **214**, 2, 1136–1150, doi: 10.1093/gji/ggy188.

Weber B., Becker J., Hanka W., Heinloo A., Hoffmann M., Kraft T., Pahlke D., Reinhardt J., Thoms H., 2007: SeisComp3 – automatic and interactive real time data processing. Geophysical Research Abstracts In EGU General Assembly, **9**, 09129.

ZAMG – Zentralanstalt für Meterologie und Geodynamik, 1987: Austrian Seismic Network. International Federation of Digital Seismograph Networks, Other/Seismic Network, doi: 10.7914/SN/OE.

sciendo

Contributions to Geophysics and Geodesy Vol. 48/4, 2018 (349–363)

Lithological composition in deep geothermal source reservoirs of temperature 160 °C in the territory of Slovakia

Vladimír BEZÁK, Dušan MAJCIN

Earth Science Institute, Slovak Academy of Sciences,
Dúbravská cesta 9, P. O. Box 106, 840 05 Bratislava, Slovak Republic;
e-mail: vladimir.bezak@savba.sk

Abstract: Our contribution presents the geological analysis results of the lithological composition for deep geothermal sources characterized by the thermal conditions suitable for application of classic hydrothermal sources exploitation and specialized EGS technologies for the electricity production in the territory of Slovakia. The results are presented in the form of lithological characterization for the isothermal surface depths with the reservoir temperature of 160 °C. The lithological conditions of geothermal source regions were constructed using available published and archive materials. From the point of view of technically utilized depths (up to 5000 m) there are two most perspective regions – Eastern Slovakia and Danube Basin with surrounding areas. We tried to characterize supposed lithological composition also in second category of geothermal sources between 5 and 6 km.

Key words: Western Carpathians, geothermal energy, lithology of deep geothermal sources

1. Introduction

The territory of Slovakia belongs to the very perspective European areas suitable for the geothermal energy exploitation (*Hurtig et al., 1992; Geoelec, 2013, 2016; Majcin et al., 2017*). The activities related to the geothermal energy sources prospection in Slovakia were devoted to some selected localities, however, there were published also global studies of the whole area of Slovakia. The existing knowledge was concentrated and analyzed mainly in the Atlas of geothermal energy of Slovakia (*Franko et al., 1995*). This very important monographic publication presents the summary of research

doi: 10.2478/congeo-2018-0017

results in the period of more than two decades of the authors and other scientists working in this subject field as well. Among other problems it evaluates also the thermal, geological and hydrological conditions for geothermal energy, thermal capacity of sources and defines basic selection of region to separate source areas. The atlas, mentioned above, brings the data and map basis for subsequent geothermal energy studies in the Slovakia.

The prospection activities and applications were aimed mainly to hydrothermal sources (*Král et al., 1985; Franko et al., 1986; Franko et al., 1995; Remšík and Bodiš, 2010; Fendek et al., 2011* and plenty of other publications from partial geothermal localities of the Slovakia). The research activities were less focused to problems of the energy acquirement by the petrothermal approaches including the HDR (hot dry rock) and HWR (hot wet rock) ones. Beside some methodologically and technically specialized works various local analyses were accomplished. They were related mainly to the structure Beša-Čičarovce (*Franko et al., 1986; Rudinec, 1989; Franko et al., 1995; Masaryk, 2008*). In the recent years some projects of geothermal energy exploitation by EGS systems were prepared in localities of both the Danube Basin and East-Slovakian Basin, however they were not realized till now.

The publications *Majcin et al. (2016, 2017)* create the optimal geothermal base for selection of areas from region under study suitable for the deep geothermal energy utilization in the electric energy production. The mentioned papers provide, among other things, the depth distributions for deep temperature of about 160 °C which is sufficient for the reasonable economic exploitation of the geothermal energy for electricity production minimally by the binary cycle technologies. This knowledge defines basic division of perspective regions both for classic hydrothermal source types and for petrothermal sources within Slovakia.

Our contribution is aimed to precision of this division by other geothermal source parameters namely geological, economic and technical ones. For defining perspective regions in addition to available depths (optimally up to 5 km, max. up to 6 km) and terrain accessibility is another important criterion lithology in the depths involved. In this work, we have therefore mainly focused on it. We used the available information from both published and archive sources (mainly results of *Franko et al., 1995; Bezák et al., 2015*) and we use them in this work as an input data.

2. Methods

The principle of the successive separation was applied for the selection of perspective areas for deep geothermal sources exploitation within the Slovakia.

The temperature of the acquired liquid medium on the Earth's surface represents the basic determining criterion. There the reservoir temperature of 160 °C is required as the smallest one for the reasonable electric energy production minimally by binary cycles (Kalina cycle, Organic Rankine cycle or others). The starting selection model is taken from the map published in *Majcin et al. (2017)*. The second criterion for the classification of geothermal source areas has technical and economical nature. It is represented by the depth at which the required reservoir temperature is safely and effectively reachable by present day drilling methods. Nowadays the depth of 5000 m is supposed as the maximum reasonable value. The third criterion for the utilization of geothermal sources of the petrothermal type is related both to the structural and lithological conditions suitable for creation of the artificial underground heat exchanger as a part of the enhanced geothermal system (EGS). The lithological situation in the depths of determined reservoir temperature is very useful also for appraisal of the existence and quality of the geothermal energy sources.

To evaluate the territory of Slovakia in terms of its lithologic composition in the depths of the 160 °C isothermal surface, we have divided it into two categories: depth up to 5 km and depth of 5–6 km. The first depth level is the most appropriate in terms of the technological reachability (in certain areas, the mentioned temperature can be found at a 3–4 km depth), morphology (lowlands and hill country) and availability of data on the expected lithology at the said depth (boreholes, geophysical data, tectonic models). The data from the individual depth levels, which can be found in the Geothermal atlas of Slovakia (*Franko et al., 1995*), are an essential source of information for our analysis of the lithologic structure. Additional data have been acquired from the deep boreholes (*Biela, 1978*). Lithology mainly of basin filling and some other complexes was taken over project Thermes (synthesis about lithology of several authors, *Bezák et al., 2015*) and explications to the Tectonic map of Slovakia (*Bezák et al., 2004*) and other sources. The geophysical data, mainly magnetic, gravimetric and

magnetotelluric (mainly *Kubeš et al., 2001; Pašteka et al., 2017*) were yet another important source of information.

The first category is divided into two areas – Eastern Slovakia and the area of the Danube Basin with the adjacent areas. Both have diverse parameters in the terms of geology. The second category (5–6 km) stretches from W to E across whole territory of Slovakia and it is least represented in Central Slovakia. The assessment of the likely lithologic composition is very ambiguous at these depths. In Western Slovakia, where the crust is thinner, we could to use also the gravimetric and magnetic results and divide the areas with predominance of granitoids and metamorphites in studied depths. Other areas are evaluated on the basis of available conceptual and factual knowledge about the tectonic structure (e.g. the Flysch Belt, Klippen Belt) or assessed as undivided crystalline complexes. An exception is the drilled Cretaceous Rochovce granite, whose impact is expected up to the required depth. The occurrence of areas with supposed subvolcanic bodies is also very interesting from the geothermic point of view.

The basic tectonic divisions of the complexes in the depths of temperature 160 °C is presented in Fig. 1. The numbers dedicate descripted areas from the second category. Two areas of first category are presented separately more in Fig. 2 and 3.

3. Results: supposed lithology of individual areas for the 160 °C isotherm

Distribution of lithological complexes for the temperature level of 160 °C is based mainly on the work of *Franko et al. (1995)*, modified after *Bezák et al. (2004)* and *Bezák et al. (2015)*. The mentioned distributiom for Danube Basin is depicted in Fig. 2 and for Eastern Slovakia in Fig. 3. Lithology description for depths 5–6 km is divided into partial areas after numbers which are drawn in Fig. 1.

The Danube Basin and surrounding areas (Fig. 2)

Danube Basin is thermally extensive and it started to open up at the end of Lower and beginning of Middle Miocene. The main part of the synrift phase occurred during the Middle Miocene, and the postrift or thermal phase took

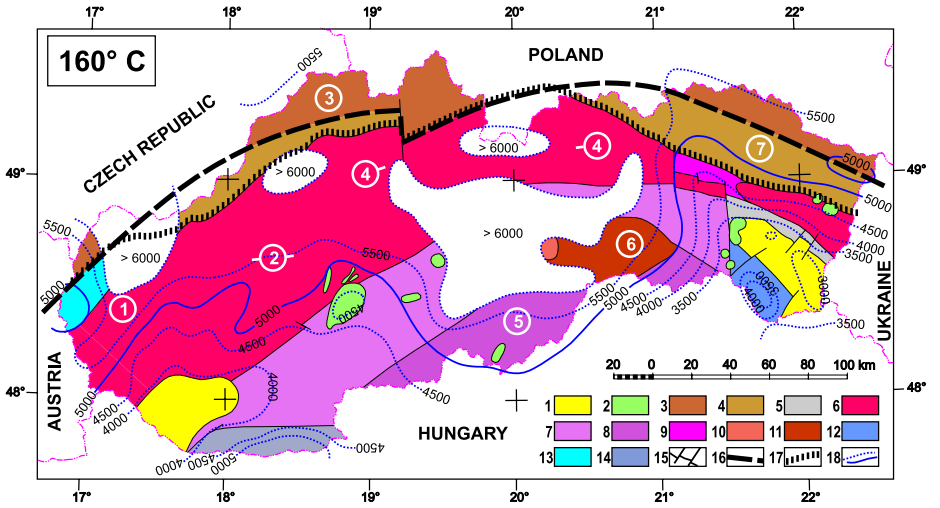

Fig. 1. Basic tectonic division of supposed rock complexes in depths demarcated by the temperature of 160 °C in the territory of Slovakia. 1 – Neogene sediments and volcanoclastics, 2 – supposed areas of subvolcanic intrusions, 3 – Flysch Belt with underlying European platform, 4 – Flysch Belt with underlying supposed Pieninic crust, 5 – Iňačevo-Kričevo unit, 6 – crystalline complexes of the Tatricum unit, 7 – crystalline complexes of the Veporicum unit, 8 – altered crystalline complexes of the Veporicum with supposed Cadomian basement, 9 – Mesozoic complexes of Fatricum, 10 – Rochovce granite, 11 – Gemericum unit with underlying Veporicum, 12 – Zemplinicum unit, 13 – Eastern Alps units, 14 – Pelsonia unit, 15 – rock complexes boundaries and faults, 16 – axis of Carpathian Conductivity Zone position, 17 – reference position of Klippen Belt, 18 – depths of the isothermal surface of 160 °C plotted with the isoline step of 500 m. Numbers in circles – described areas of second category (between 5–6 km).

place during Upper Miocene and Pliocene. The history of this basin started by arching out of the bedrock and erosion of the younger, particularly Mesozoic complexes. This was linked with the growth of asthenolite, which subsequently fused into the crust, but also resulted in subsidence, heat flow and volcanism. The biggest depression, and also thickness of sedimentary filling can be found in the central part (Gabčíkovo depression). Here, the 160 °C isotherm is usually 4 km below the surface or higher and thus in the Neogene sediments.

The sedimentation was accompanied by volcanism. Apart from the typical sedimentary rocks of pelitic and psammitic origin (mostly sandstone and claystone), the sedimentary fill of the basin is also composed of the

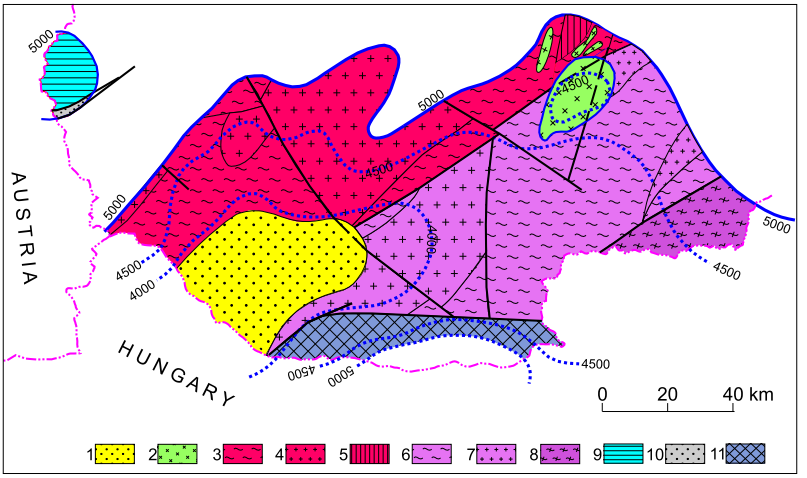

Fig. 2. Lithological complexes on the isotherm lying in the depth up to 5 km in the area of Danube Basin. 1 – Neogene sediments and volcanoclastics, 2 – supposed areas of subvolcanic intrusions, 3 – metamorphic complexes of the Tatricum unit, 4 – granitoid complexes of the Tatricum unit, 5 – Tatric mostly Mesozoic cover unit, 6 – metamorphic complexes of the Veporicum unit, 7 – granitoid complexes of the Veporicum unit, 8 – altered crystalline complexes of the Veporicum with supposed Cadomian basement, 9 – Eastern Alps Mesozoic units, 10 – Eastern Alps Palaeozoic units, 11 – Pelsonia unit.

rocks of volcanic origin (mostly volcanoslastics, but also lava flows and extrusions). Products of volcanism are concentrated mainly in the eastern and north-eastern edge of the basin, and are also buried under the younger basin fills. Their position is captured mainly by magnetic measurements and the largest occurrences are shown in the Tectonic Map of Slovakia (*Bezák et al., 2004*). The products of magmatism are shown also in the magnetic maps as positive anomalies. The Danube Basin is characterized by a relatively large number of positive anomalies (*Kubeš et al., 2010*). The sources of these anomalies are found not only in the sedimentary-volcanic complex of the Tertiary period, but also in the Pre-Tertiary basement. The anomalies in the basement can be caused by the basal differentials of granitoids (granodiorites, diorites, tonalites), amphibolites and some types of metamorphic rocks (e.g. mica schists).

In the remaining parts of the basin and neighbouring volcanic mountains, the isotherm 160 °C decreases to the bedrock at a depth of 4–5 km. In these depths, the bedrock already consists exclusively of Palaeozoic metamorphic

and magmatic rocks with the exception of a small area in NE (Žiarska kotlina depression), where is a probable occurrence of Mesozoic carbonates and subvolcanic intrusions. In the area of large stratovolcanoes, such as Banská Štiavnica stratovolcano, the occurrence of intrusive volcanic rocks mostly of intermediary composition (diorites, porphyrites) is highly probable.

Metamorphic rocks of all types, ranging from phyllites to gneisses, are present. The drilling exploration and geophysical analysis indicate that relatively large areas in the Danube Basin basement are expected to include magmatic granitoid rocks of Palaeozoic age. The metamorphic and magmatic complexes belong to three tectonic units – Tatricum, Veporicum and Pelsonia. The southern part of the Veporicum is greatly altered because of the effects of volcanic and hydrothermal processes and it may have different physical properties – we therefore visualize it separately. The Pelsonia unit is located south of the Hurbanovo fault, with a possible highly-metamorphic Cadomian basement with an early Palaeozoic sedimentary cover mainly composed of carbonates. In the southernmost area, the isotherm 160 °C again falls below the depth 5 km, which is caused most likely by the occurrence of Pelsonia carbonates.

Outside the territory of Danube Basin temperatue isoline 160 °C lying in the depth smaller than 5 km also is located in small zone in the NW of the Vienna Basin. In these depths most authors expect the Mesozoic complexes of the Eastern Alps provenance. Carbonates are the prevalent lithological types here. In a small section, there are traces of metasediments of the Grauwacken zone of the Eastern Alps.

Area of the Eastern Slovakia with the isotherm 160 °C in the depth less than 5 km (Fig. 3)

The highest isotherm 160 °C in Slovakia exists in the East-Slovakian Basin, which is the center of this general area. Here the depth of the isoterm position is usually smaller than 3500 m and some times even less than 3000 m. The East-Slovakian Basin had a very specific tectonic development (e.g. *Rudinec, 1989; Bezák et al., 2004*). The bedrock of the basin is broken into blocks with uneven depth, with the deepest parts of more than 6 km in the central depression of the NW direction. The isotherm lies in the Neogene sedimentary-volcanic filling in most parts of the basin.

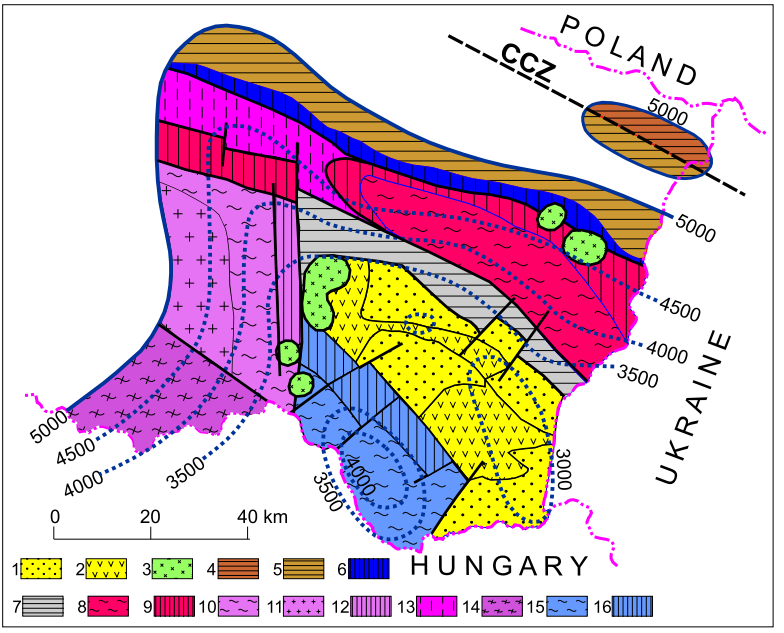

Fig. 3. Lithological complexes on the isotherm lying in depth up to 5 km in the area of the Eastern Slovakia. 1 – Neogene sediments, 2 – Neogene volcanoclastics, 3 – supposed areas of subvolcanic intrusions, 4 – Flysch Belt with underlying European platform, 5 – Flysch Belt with underlying supposed Pieninic crust, 6 – Klippen Belt, 7 – Iňačevo-Kričevo unit, 8 – crystalline complexes of the Tatricum unit, 9 – Mesozoic cover of Tatricum, 10 – metamorphic complexes of the Veporicum unit, 11 – granitoid – complexes of the Veporicum unit, 12 – Mesozoic cover of Veporicum, 13 – Mesozoic complexes of Fatricum, 14 – altered crystalline complexes of the Veporicum with supposed Cadomian basement, 15 – crystalline complexes of Zemplinicum unit, 16 – Upper Palaeozoic and Mesozoic cover of Zemplinicum.

The filling of East-Slovakian Basin consists of Neogene sediments and volcanics (from Lower Karpathian to Late Panonian and Pontian age). The sandstones, conglomerates, siltstones, claystones and different volcanoclastics are the prevailing lithological types (*Vass et al., 1991*).

Volcanic activity occurred in parallel with the sedimentation in the Miocene period not only in the neighbouring volcanic mountains but also in the potential centers in the basin. The volcanic centers within the basin fill are bound to the volcanic-tectonic zones in the NW–SE direction, which are marked on the Tectonic Map of the Slovakia (*Bezák et al., 2004*). The mag-

netic map (*Kubeš et al., 2001*) also shows the buried volcanoes. Therefore, the volcanic sedimentation is frequent and sometimes dominant. In the area of the volcanic centers we can assume the occurrence of subvolcanic intrusions in the depths of interest with a temperature of 160 °C.

The isotherm 160 °C falls below 4 km on the edges of the basin and it enters to the bedrock of the Neogene sediments and the Slánske vrchy Mts. volcanites. The composition of the bedrock is varied in view of the tectonically complicated interface of the Eastern and Western Carpathian units.

The geological and tectonic composition of the Pre-Tertiary bedrock in the East-Slovakian Basin is greatly affected by the deeply-established Slanská tectonic line, which was defined by *Slávik (1974)*. It stretches in a north-south direction under Slanské vrchy Mts. and it allowed the extrusion of volcanic material to the surface. It serves as a contact area for the Gemericum and Veporicum unit in the west with the Zemplín and Iňačevo-Kričevo units. The situation east of the Slanska fault system is geologically and tectonically complicated. Mesozoic complexes (mostly carbonatic) of the Fatricum is located in the northern part of the territory, it is surrounded by the southern edge of the Klippen Belt and it emerges on surface in the Humenské vrchy hills. In this part of basement we assumed also (*Franko et al., 1995*) crystalline complexes of the Tatricum. We expect that the Iňačevo-Kričevo unit is located to the South of Fatricum and Tatricum in the Neogene sedimentary bedrock, and composed of very weakly metamorphic fine sandstones and schists with pockets of limestones.

The Zemplinicum tectonic unit is located in the southern part of this territory (*Slávik, 1976*). Zemplinicum is a structural-tectonic unit composed of highly metamorphic crystalline core (mostly gneisses and amphibolites) and their Carboniferous-Permian and Mesozoic cover. The tectonic structure of the Zemplinicum rock complexes is not entirely clear to this day. The western part of the said territory is composed of crystalline complexes of the Veporicum with a significant presence of granitoids. Numerous authors (e.g. *Franko et al., 1995*) expect the occurrence of Mesozoic carbonates in the cover of crystalline complexes.

The isotherm 160 °C reaches the outer flysch sediments (sandstone, claystone) in the northernmost part of the area in question. We assume that these flysch sediments are situated on the boundary of supposed Pieninic crust and European platform.

The territory of Slovakia with the isotherm 160 °C in a depth of 5–6 km

This territory stretches across the whole Slovakia from west to east. It occupies various geological and geomorphological units, which will be described sequentially from the west as presented and numbered in Fig. 1. The smallest area is located in Central Slovakia where the isothem falls below 6 km mostly under the higher mountains. Supposed lithology is described after smaller regions marked by numbers which are shown in Fig. 1.

1. Area of the SE part of the Vienna Basin and the Malé Karpaty Mts.

In the said depth, the basement of Vienna Basin also includes the Mesozoic East Alpine complexes in the north, while in the southern part and in the area of the Malé Karpaty Mts. we can already see the complexes of the Tatricum represented by Hercynian metamorphites (paragneisses, amphibolites, phyllites). The occurrence of granitoids is likely to be the case in these depths mostly SE of the Malé Karpaty Mts. which means that this area is more favourable in terms of lithology and morphology. The occurrence of flysch sediments is possible even at a depth of more than 5 km in the northern part up to the CCZ axis. The flysch sediments in the northernmost part of Vienna Basin basement are thrusted onto the Brunia crystalline structures and/or their Palaeozoic cover, which mainly consists of carbonates.

2. Area of the northern protrusions from the Danube Basin, including the Piešťany and Horná Nitra depressions and the surrounding mountains of Považský Inovec and Tribeč

At a depth of 5–6 km, we mainly expect the Tatricum crystalline rocks in this area. Due to the reduced crust thickness in this area as a result of asthenolite, the gravimetric data allow us to distinguish the position of the predominantly heavier Palaeozoic metamorphic rocks (gneisses, micaschists, less phyllites and amphibolites) in the mountains area from the lighter granitoids in the depressed areas – basins, coupled also with the effects of overlying Tertiary sediments. In some tectonically exposed areas, for example along the Považie fault or near the Klippen Belt, we can consider the possibility of Mesozoic and Upper Palaeozoic rocks being tectonically sucked into these depths (see *Franko et al., 1995*). The Mesozoic rocks are mainly represented by the carbonates of the cover of crystalline complexes

and Fatricum units.

3. Outer Carpathian Flysch Belt in the north-western Slovakia

This is a Flysch Belt where the flysch sediments may be assumed to have reached a thickness of more than 5 km mainly in the southern part, near the Klippen Belt zone. These lighter sediments overshadow the weight effect of the European platform in the bedrock. In these areas, the European platform is represented by the Brunia unit consisting of granitoids, gneisses and amphibolites and their Lower Palaeozoic cover. The span and mainly the extent of particular Klippen Belt rocks (carbonates, marbles, schists, sandstones etc.) in the depth is difficult to assess, but their occurrence is likely in the narrow zone at the foreland of the Tatricum. Some authors even consider a larger presence of Mesozoic rocks of the oceanic type. In the areas where the Klippen Belt zone passes south of the Carpathian Conductivity Zone (CCZ), we assume the presence of the segment of Pieninic crust in the bedrock of flysch sediments, which has a rock composition similar to Brunia.

4. Northern Slovakia: area of core mountains from Strážovské vrchy Mts. to Branisko Mts. and the adjacent basins or hills with a predominant Tertiary sediments

In this areas the isotherm 160 °C lies in the depth more than 5500 m, thats why these areas only contain Palaeozoic crystalline rocks, mostly of Tatricum, less of Veporicum tectonic unit. However, since this area belongs to the Carpathian gravity low, we are lacking the distinctive features for the determination of the position of granitoids and metamorphic rocks. The geological development on the surface indicates that granodiorites and granites prevail along with orthogneisses and paragneisses with smaller content of amphibolites.

5. Wider area of the Lučenská kotlina depression

In the mentioned depth range, the Veporicum crystalline rocks prevail in the northern part, and due to the Hercynian tectonic superposition, we expect this area to contain mainly Palaeozoic mica-schist rocks with supposed Cadomian basement in the southern part. According to the magnetotelluric measurements, the southern part exhibits anomalous conductivity along the

entire cross-section of the crust. This is due to the fact that it is substantially altered by intensive tectonic movements in the regional faults and also by young volcanic activity accompanied by hydrothermal alterations. Therefore, this block is visualized separately in the Fig. 1. The occurrence of subvolcanic intrusions mostly of basaltic character is also very likely in this area.

6. Area of Gemeric unit

The occurrence of Veporicum crystalline rocks is very likely in these depths over 5500 m although the occurrence of Palaeozoic low metamorphic phyllites, metasandstones and metavolcanites of the Gemericum is also possible. The presence of a Mesozoic cover from the Veporicum is less likely. Further north, only the crystalline Veporicum is present (granitoids and metamorphites), which is tectonically separated from the Tatricum. *Franko et al. (1995)* again expects the possible presence of carbonate complexes of the Tatricum cover in the areas adjacent to Klippen Belt, as well as Fatricum complexes. Relatively small intrusion of the Cretaceous Rochovce granite on the western edge of Gemericum is very interesting in terms of lithology.

7. Outer Carpathian Flysch Belt in the north-eastern Slovakia

This area of Outer Flysch Belt has a completely different gravimetric but also magnetotelluric features than the western flysch area. Lithology of flysch sediments is same (alternation of sandstones and claystones). We assume that this is caused by a different crust type in the bedrock of the flysch sediments (tectonically disturbed platform, e.g. *Bezák et al., 1997*, segment of Pieninic crust, e.g. *Grad et al., 2006*) and especially by a much larger influence of the volcanic activity (intrusions into the flysch are also expected, see *Kucharič et al., 2012, 2013*), including the protrusions of partial asthenolites into the flysch strata. Therefore, this area is interesting and promising in terms of geothermal use.

4. Conclusion

The contribution finalizes the primary selection of the perspective areas for deep geothermal sources exploitation within the studied region of Slovakia.

We utilized the principle of the successive separation on the geothermal base (*Majcin et al. 2017*) which provides the depth distributions for deep temperature of about 160 °C. This temperature is sufficient for the reasonable economic exploitation of the geothermal energy for electricity production minimally by the binary cycle technologies. Applied were additional geological, economic and technical parameters of geothermal sources.

In this paper we described the supposed lithological composition in depths technically applicable for utilization of the heat of rock complexes. The studied territory of Slovakia is divided to two categories according depths – first one up to 5 km and the second one between 5 and 6 km. The results were constructed from various accessible geoscientific sources enhancing the basic knowledge presented in Geothermal atlas (*Franko et al., 1995*). The rock complexes are presented only schematically because of better lucidity. Our results create the base for both starting decisions of regions suitable for electricity production by binary cycles and further selection requires more precise exploratory development works (analysis of geological profiles, boreholes, additional geophysical works and others) in concrete localities. According the basic parameters (temperatures, depth, accessibility, lithology) application by geothermal sources evaluation we determined the central parts of both basins (East-Slovakian and Danube) as the most favourable. The suitability is increased mainly in the case if the sedimentary filling containes volcanic bodies. Further we incorporate the border parts of mentioned basins including the volcanic mountains, from intramountains basins Žiarska kotlina depression is favourable, further NE part of Outher Carpathians Flysch zone and a part of Vienna Basin to the perspective geothermal areas of Slovakia for electricity production.

Acknowledgements. The authors are grateful for partial support of the work by the APVV agency by means of project APVV-0724-11 and the Slovak Grant Agency VEGA by means of projects 2/0091/15, 2/0042/15 and 1/0141/15.

References

Bezák V., Šefara J., Bielik M., Kubeš P., 1997: Models of the Western Carpathian Litosphere. In Grecula P., Hovorka D., Putiš M.: Geological evolution of the Western Carpathians. Geocomplex, 24-34, ISBN 80-967018-7-8, 95/5305/418.

Bezák V., Broska I., Ivanička J., Reichwalder P., Vozár J., Polák M., Havrila M., Mello J., Biely A., Plašienka D., Potfaj M., Konečný V., Lexa J., Kaličiak M., Žec B., Vass D., Elečko M., Janočko J., Pereszlényi M., Marko F., Maglay J., Pristaš J., 2004: Tectonic map of Slovak Republic (Tektonická mapa Slovenskej republiky). Vydavateľstvo ŠGÚDŠ, Bratislava (in Slovak).

Bezák V., Hók J., Král M., Kucharič Ľ., Šipka F., Šujan M., Vitáloš R., Vranovská, A., 2015: Lithological and tectonic characteristic of areas in Slovakia potentialy suitable for utilization of Hot Dry Rock (in Slovak). In: Bezák V. et al. (eds.): Structure and thermal state of the West Carpathian lithosphere: hot dry rock energy sources potential of Slovakia. Earth Science Institute, SAS, Bratislava, 125–139.

Biela A., 1978: Deep boreholes in covered areas of the Inner Western Carpathians (Hlboké vrty v zakrytých oblastiach vnútorných Západných Karpát). Regionálna geológia Západných Karpát, 10, 11, GÚDŠ, Bratislava, 224 p. (in Slovak).

Fendek M., Bágelová A., Fendeková M., 2011: Geothermal energy world-wide and in Slovakia. Podzemná voda, XVII, 1, 74–83 (in Slovak).

Franko O., Fusán O., Král M., Majcin D., 1986: Distribution of high and middle temperature geothermal waters and hot dry rock in Slovakia. In: Geothermal energy of Slovakia and their utilization. Dionýz Štúr Institute of Geology, Bratislava, 81–92 (in Slovak).

Franko O., Fusán O., Král M., Remšík A., Fendek M., Bodiš D., Drozd V., Vika K., 1995: Atlas of Geothermal Energy of Slovakia, Dionýz Štúr Institute of Geology, Bratislava, 1–194.

Geoelec, 2013: A prospective study on the geothermal potential in the EU. Electronic source: `http://www.geoelec.eu/wp-content/uploads/2011/09/D-2.5-GEOELEC-prospective-study.pdf`.

Geoelec, 2016: Geothermal Potential for Electricity Generation for the EU. 2016. Interactive GIS map. Electronic source: `http://www.thermogis.nl/geoelec/ThermoGIS_GEOELEC.html`.

Grad M., Guterch A., Keller G. R., Janik T., Hegedűs E., Vozár J., Ślaczka A., Tiira T., Yliniemi J., 2006: Lithospheric structure beneath trans-Carpathian transect from Precambrian platform to Pannonian basin CELEBRATION 2000 seismic profile CEL05. J. Geophys. Res., **111**, B03301, `doi: 10.1029/2005JB003647`.

Hurtig V., Čermák V., Haenel R., Zui V.l., 1992: Geothermal Atlas of Europe. Hermann Haack, Geogr.-Kart. Anstalt, Gotha, (Enclosure maps).

Král M., Lizoň I., Jančí J., 1985: Geothermal exploration of SSR (Geotermický výskum SSR). Manuscript, Geofyzika Bratislava, 1–116 (in Slovak).

Kubeš P., Bielik M., Daniel S., Čížek P., Filo M., Gluch A., Grand T., Hrušecký I., Kucharič Ľ., Medo S., Pašteka R., Smolárová H., Šefara J., Tekula B., Ujpál Z., Valušiaková A., Bezák V., Dublan Š., Elečko M., Határ J., Hraško Ľ., Ivanička J., Janočko J., Kaličiak M., Kohút M., Konečný V., Mello J., Polák M., Potfaj M., Šimon L., Vozár J., 2001: Atlas of geophysical maps and profiles (Atlas geofyzikálnych máp a profilov). Manuskript, Geofond, ŠGÚDŠ Bratislava (in Slovak).

Kubeš P., Bezák V., Kucharič Ľ., Filo M., Vozár J., Konečný V., Kohút M., Gluch A.,

2010:Magnetic field of the Western Carpathians (Slovakia): reflection structure of the crust. Geol. Carpath., **61**, 437–447.

Kucharič Ľ., Bezák V., Majcin D., Vozár J., 2012: Carbonate complexes underlying Flysch belt and subsurface Neogene volcanic in the NE part of Slovakia – a potential for geothermal energy and raw materials In: Contributions to Geophysics and Geodesy. ISSN 1335–2806, **42**, 4, 283–294.

Kucharič Ľ., Bezák V., Kubeš P., Konečný V., Vozár J., 2013: New magnetic anomalies of the Outer Carpathians in NE Slovakia and their relationship to the Carpathian Conductivity Zone, Geological Quaterly, **57**, 1, 123–134, doi: 10.7306/gq.1079.

Majcin D., Král M., Bilčík D., Šujan M., Vranovská A., 2017: Deep geothermal sources for electricity production in Slovakia: thermal conditions. Contrib. Geophys. Geod., **47**, 1, doi: 10.1515/congeo-2017-0001.

Majcin D., Kutas R., Bilčík D., Bezák V., Korchagin I., 2016: Thermal conditions for geothermal energy exploitation in the Transcarpathian depression and surrounding units. Contrib. Geophys. Geod., **46**, 1, 33–49.

Masaryk M., 2008: Energetic potential of dry rock geothermal heat in the region of Slovakia and the utilization for electric energy production (Energetický potenciál geotermálneho tepla suchých hornín na území Slovenska a jeho využitie pre výrobu elektrickej energie). Slovak University of Technology, Bratislava, 20 p. ISBN: 978802 273090. (in Slovak)

Pašteka R., Zahorec P., Kušnirák, D., Bošanský M., Papčo J., Szalaiová V., Krajňák M., Marušiak I., Mikuška J., Bielik M., 2017: High resolution Slovak Bouguer gravity anomaly map and its enhanced derivative transformations: new possibilities for interpretation of anomalous gravity fields. Contributions to Geophysics and Geodesy, **47**, 2, 81–94.

Remšík A., Bodiš D., 2010: Geothermal waters, situation and possibilities of their utilization in Slovakia (Geotermálne vody, stav a možnosti využitia na Slovensku). ŠGÚDŠ, Bratislava, Manuscript, 19 p. (in Slovak).

Rudinec R., 1989: Crude oil, natural gas and geothermal energy resorces in Eastern Slovakia (Zdroje ropy, zemného plynu a geotermálnej energie na Východnom Slovensku). ALFA, Bratislava, 162 p. (in Slovak with english summary).

Slávik J., 1974: Volcanism, tectonic and mineral deposits of the East Slovak Neogene and its position in the Neoeurope (Vulkanizmus, tektonika a nerastné suroviny neogénu východného Slovenska a pozícia tejto oblasti v Neoeurópe). Thesis, Geofond Bratislava, 1–341 (in Slovak with Russian and English summary).

Slávik J., 1976: Zemplinicum – a possible new tectonical unit of the central Carpathians (Zemplinikum – možná nová tektonická jednotka centrálnych Karpát). Geologické práce, Správy, **65**, 7–19.

Vass D, Cverčko J., Elečko M., Kaličiak M., Mořkovský M., Vozár J., 1991: Stripped geological map of East-SLovakian lowlands, scale 1:100000 (Odkrytá geologická mapa Východoslovenskej nížiny 1:100000). GÚDŠ, Bratislava.